STANFORD
AERONAUTICS &
ASTRONAUTICS

AA103
Air and Space Propulsion

Chapter 11 - Hybrid Rockets

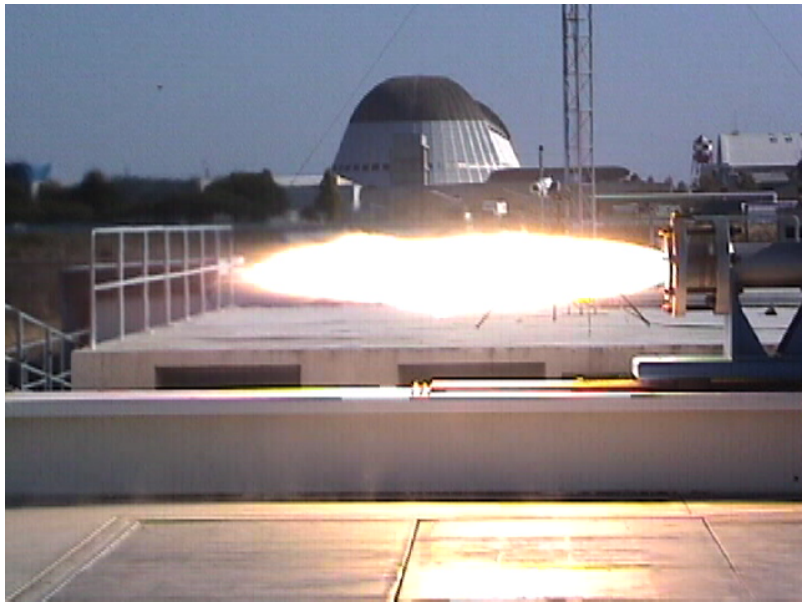

STANFORD
AERONAUTICS & ASTRONAUTICS

All modern launch systems use conventional solid and/or liquid rocket propulsion systems

Liquid Main Engines

High performance and throttle-able but complex, expensive, explosion hazard.

Worldwide both liquid and solid rocket propulsion systems fail at a rate of about 2.5 per 100 launches. The US failure rate is about 1.5 per 100. No other industry accepts this rate of failure.

Reference: I-Shih Chang and Edmardo Joe Tomei of the Aerospace Corp. AIAA paper 2005-3793

Solid Rocket Booster

Mechanically simple but difficult to throttle, expensive, explosion hazard, environmental hazard.

There are Increasing concerns about groundwater contamination by perchlorates produced in the manufacture of solid rocket propellants. Even very low levels of contamination are correlated with reduced iodine intake in women.

Reference: CDC Report doi:10.1289/ehp.9466 October 5, 2006. Available at http://dx.doi.org/

Hybrid Rocket System

A hybrid rocket is a design where a liquid oxidizer is vaporized and passed over a solid fuel.

An igniter is used to evaporate some of the fuel and initiate combustion. Once a flame is established over the fuel surface the process is self-sustaining.

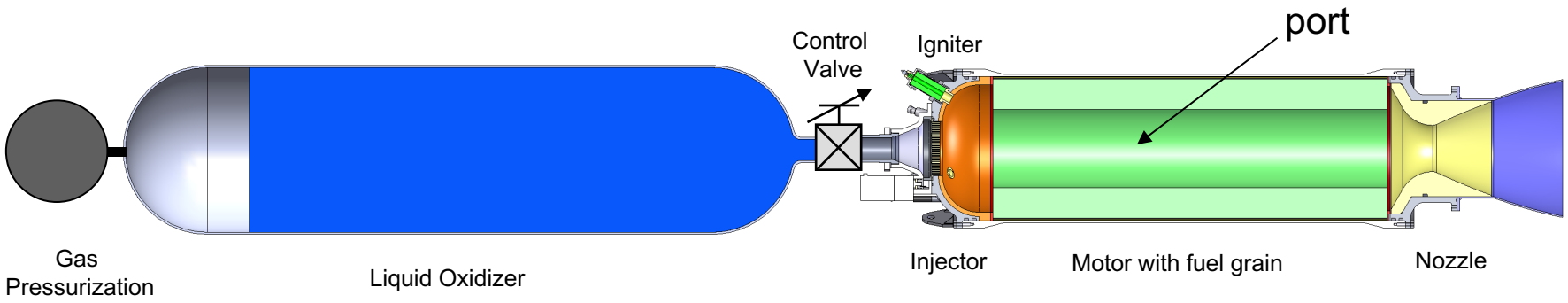

The hybrid rocket offers an inherently safe, mechanically simple alternative with lower life cycle costs compared to solids and liquids.

Why hybrids ??

The Challenger disaster - January 28, 1986

$t + 0.678\,\text{sec}$

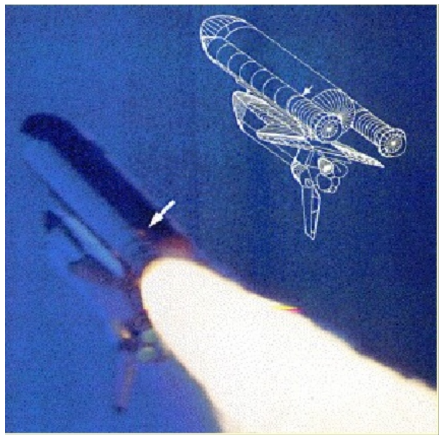

$t + 59\,\text{sec}$

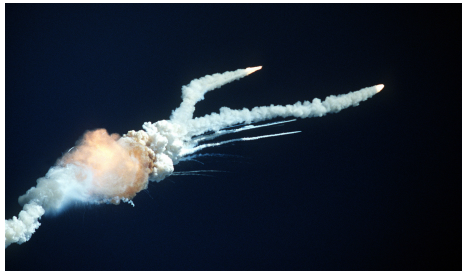

$t + 60\,\text{sec}$

Titan IVA
7-Segment SRM
First Launch: 6/14/1989

Wp = 591,000-lb/SRM
F_{Vac} = 1,600,000-lb/SRM
Burn time = 120-sec

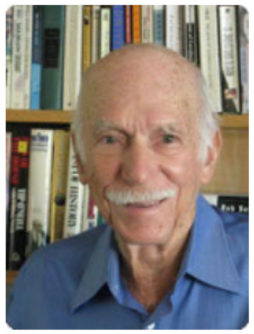

Dave Altman
Vice pres CSD, Ret.

In the middle of all this was Dave Altman, now almost 100, of Menlo Park. A member of the Rogers commission, a founder of CSD and one of the inventors of segmented solid boosters, Dave is one of the earliest proponents of safer, cheaper, throttleable hybrids.

CSD's Development & Test Facility in Coyote Valley (about 5,400 acres), also serving as a game reserve for elk, deer, mountain lions, bobcats, coyotes, wild boar and many birds

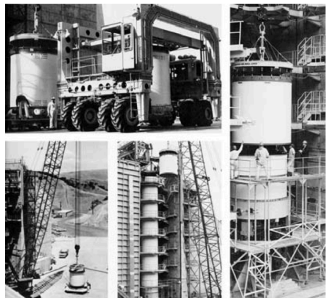

Titan booster build-up and aerial view of static test at CSD's ST-9 vertical test stand

Titan 34D-9 SRM failure - April 18, 1986

STANFORD
AERONAUTICS & ASTRONAUTICS

On August 17, 1933, the first liquid rocket launch of the Soviet Union was a hybrid that used gelled gasoline and liquid oxygen.

Soviet rocket pioneer M.K. Tikhonravov and the GIRD-9.

In 1933 the first Soviet hybrid-propellant rocket, designed by M. K. Tikhonravov and built by the Korolev team, was launched at the Nakhabino test range.

The takeoff weight of the 2.4-meter-long rocket was 19 kg; its propellant weight—5kg; the engine produced a thrust of 25 to 33 kg; its thrust chamber pressure ranged from 5 to 6 atmospheres. The engine used liquid oxygen delivered into the chamber under the pressure of its own vapours, and solidified gasoline which was placed in the combustion chamber (1 to 1.5 kg.). It was fired from a vertical ramp. During the first trial launching on August 17, 1933, it reached a height of aobut 400 meters before the combustion chamber burned through. The flight lasted 18 seconds. During the second launching (autumn 1933) the rocket reached an estimated height of 100 meters when the engine exploded. In 1934 the rocket underwent several successful trials and reached a height of 1,500 meters.

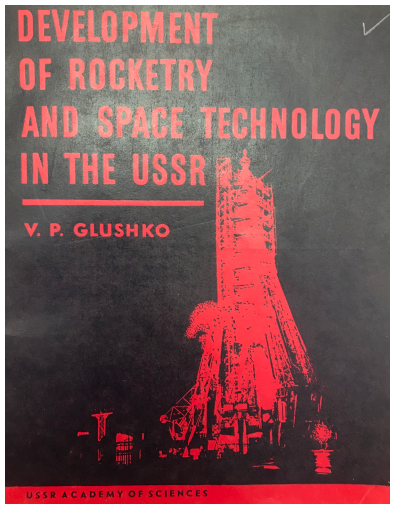

STANFORD
AERONAUTICS &
ASTRONAUTICS

Peregrine Motor - NASA Ames

Some history of hybrids- (1960 - 1985)

- 1960's: Extensive research at various companies.
  - Chemical Systems Division of UTC
    - Modeling (Altman, Marxman, Ordahl, Wooldridge, Muzzy etc…)
    - Motor testing (up to 40,000 lb thrust level)
  - LPC: Lockheed Propulsion Company, SRI: Stanford Research Institute, ONERA (France)

- 1964-1984: Flight System Development
  - Target drone programs by Chemical Systems Division of UTC
    - Sandpiper, HAST, Firebolt
  - LEX Sounding Rocket (ONERA, France)
  - FLGMOTOR Sounding Rocket (Sweden)

- 1973-1982: Indian Institute of Science 100 kgf motor
  - Swirl injection, hypergolic solid fuels with RFNA
  - 96% c* efficiency

CSD's Li/LiH/PBAN-F_2/O_2 Hybrid
Measured Isp=480 sec

Firebolt Target Drone

Recent History - (1981 - Present)

- 1981-1985: Starstruck Co. launched the Dolphin sounding rocket (35 klb thrust)
- 1985-1995: AMROC continuation of Starstruck
  - Tested 10, 33, 75 klb thrust subscale motors.
  - Developed and tested the H-1800, a 250 klb LO_2/HTPB motor.
- 1990's: NASA Hybrid Propulsion Development Program (HPDP)
  - Developed and tested 250 klb thrust LO_2/HTPB motors.
- 2002: Lockheed developed and flight tested a 24 inch LO_2/HTPB hybrid sounding rocket (HYSR). (60 klb thrust)
- 2003: Scaled Composites and SpaceDev developed N_2O/HTPB hybrid for the sub-orbital vehicle SpaceShipOne. (20 klb thrust)
- 2013: April 29 First powered flight of Space Ship Two
- 2018: September 27 – Nammo launch of the Nucleus Sounding Rocket over 100km
- 2019: February 22 Virgin Galactic flight of VSS Unity with its first passenger.

Faenza, M. G., Boiron, A.J., Haemmerli, B. and O. Verberne, "The Nammo Nucleus Launch", *AIAA 2019-4049, P&E, Indianapolis, Aug 19, 2019.*

Dolphin

AMROC Motor Test

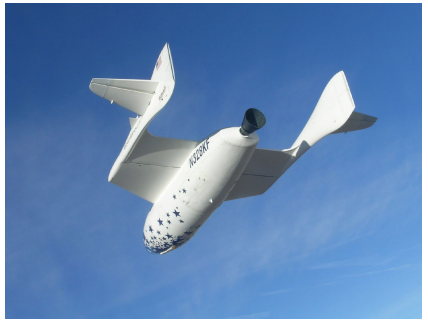

SpaceShipOne

VSS Unity

Hybrid combustion model

Turbulent boundary layer combustion

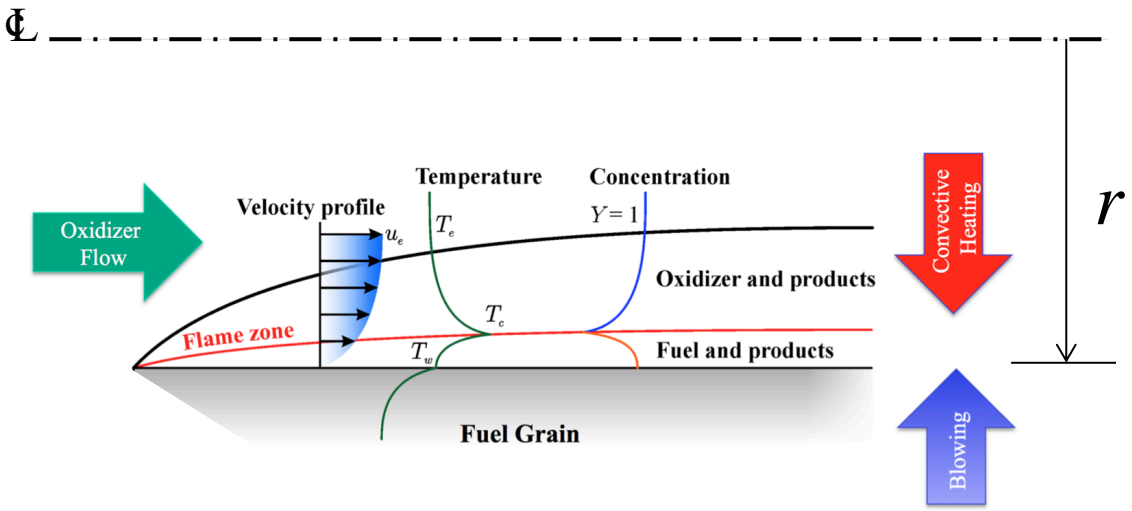

Marxman, G. A., and Gilbert, M., "Turbulent Boundary Layer Combustion in the Hybrid Rocket", *Ninth Symposium (International) on Combustion*, The Combustion Institute, pp. 371-383, 1963.

In a hybrid rocket, the fuel surface regression rate is determined by the mass flux in the port.

$$\dot{r} \approx aG^n \qquad G = \frac{\dot{m}_{port}}{\pi r^2} = \frac{\dot{m}_{ox} + \dot{m}_{fuel}}{\pi r^2}$$

Constants a and n are empirical values for a given choice of fuel and oxidizer. Typically $0.4 < n < 0.8$.

In a solid rocket the propellant surface regression rate is determined by the chamber pressure.

$$\dot{r} = aP^n$$

The constant a, depends on propellant temperature at launch, $n < 1$ is required to prevent explosion.

Hybrid motor gas generation is governed by two coupled, first order semi-impirical PDEs

Fuel surface regression rate equation

$$\frac{\partial r(x,t)}{\partial t} = \frac{a}{x^m}\left(\frac{\dot{m}_{port}}{\pi r^2}\right)^n$$

$$\dot{m}_{port} = \dot{m}_{ox} + \dot{m}_f$$

The dependence on x arises from a turbulent boundary layer heat transfer mechanism.

Port mass flow growth rate equation

$$\frac{\partial \dot{m}_{port}(x,t)}{\partial x} = \rho_f (2\pi r)\frac{a}{x^m}\left(\frac{\dot{m}_{port}}{\pi r^2}\right)^n$$

These equations are often simplified to

$$\dot{r} = aG_{ox}^n \qquad G_{ox} = \frac{\dot{m}_{ox}}{\pi r^2}$$

This can be used to roughly characterize a given motor if the O/F is not too low.

- The empirical constants a, n and m hide a variety of physical processes that affect the fuel regression rate and need to be taken into account in a given motor design. This includes
  - Radiative heat transfer
  - pyrolysis
  - two phase flow
  - turbulent and transitional flow
  - injector geometry, swirl
  - Motor/port geometry and size
- *The potential benefits of hybrids together with the complex multi-physics nature of hybrid rocket combustion make the subject an important area for both fundamental and applied research.*
- *Some good review sources,*

H. S. Mukunda, V.K. Jain, and P.J. Paul, "A review of hybrid rockets: present status and future potential", Proc. Indian Acad. Sci., Vol C 2, part 1, May 1979, pp. 215-242.

D. Altman, A. Holzman, Overview and history of hybrid rocket propulsion, in: K. Kuo, M. Chiaverini (Eds.), *Fundamentals of Hybrid Rocket Combustion and Propulsion*, Vol. 218 of Progress in Astronautics and Aeronautics, AIAA, 2007, pp. 1–36.

Chemical Rocket Propulsion: A Comprehensive Survey of Energetic Materials, Part VI Hybrid Rocket Propulsion. L. De Luca, T. Shimada, V.P. Sinditskii, M. Calabro (Editors), Springer Aerospace Technology, 2017.

STANFORD
AERONAUTICS &
ASTRONAUTICS

Port ballistic calculations

The fuel regression rate law

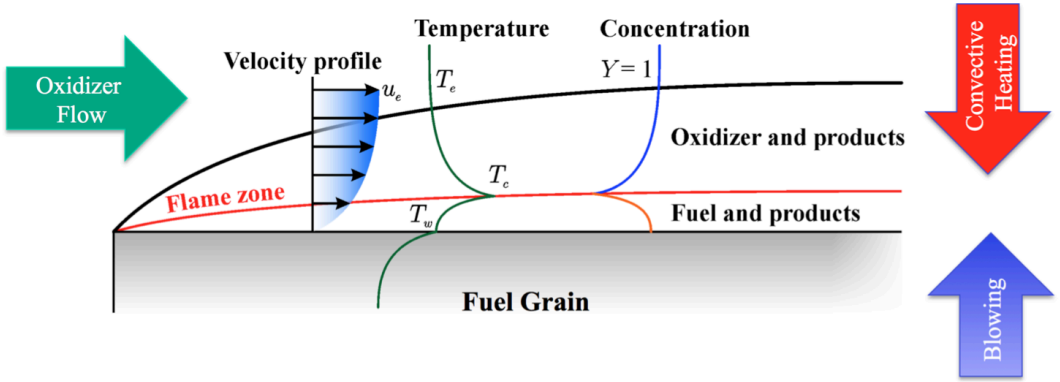

Hybrid combustion is governed by two coupled first order PDEs $\dot{m}_{port} = \dot{m}_{ox} + \dot{m}_f$

$$\frac{\partial r(x,t)}{\partial t} = \frac{a}{x^m}\left(\frac{\dot{m}_{port}}{\pi r^2}\right)^n$$

Fuel surface regression rate equation

$$\frac{\partial \dot{m}_{port}(x,t)}{\partial x} = \rho_f (2\pi r)\frac{a}{x^m}\left(\frac{\dot{m}_{port}}{\pi r^2}\right)^n$$

Port mass flow growth rate equation

The port mass flux is generally denoted by G.

$$G = \frac{\dot{m}_{port}}{\pi r^2} = \frac{\dot{m}_{ox} + \dot{m}_f}{\pi r^2}$$

The constants a, n and m are empirical values for a given choice of fuel and oxidizer. Typically m is very small and $0.4 < n < 0.7$.

$$[a] = \frac{Length^{2n+m+1}}{Mass^n Time^{1-n}}$$

The units of the regression rate constant *a*

$$\dot{r} = \frac{a}{x^m} G^n$$

$$\frac{L}{T} = \frac{[a]}{L^m}\left(\frac{M}{L^2 T}\right)^n \qquad [\ ] = \text{units of}$$

$$[a] = \frac{L^{2n+m+1}}{T^{1-n} M^n}$$

Unit conversion cgs to mks

$$a = 0.0488\left(\frac{cm^{2n+m+1}}{\sec^{1-n} gm^n}\right) = 0.0488\left(\frac{(0.01m)^{2n+m+1}}{\sec^{1-n}(0.001kg)^n}\right) = 0.0488\left(\frac{(0.01)^{2n+m+1}}{(0.001)^n}\right)\left(\frac{m^{2n+m+1}}{\sec^{1-n} kg^n}\right)$$

$$n = 0.62$$

$$m = 0$$

$$a = 0.0488\left(\frac{cm^{2.24}}{\sec^{0.48} gm^{0.62}}\right) = 0.0488\left(\frac{(0.01)^{2.24}}{(0.001)^{0.62}}\right)\left(\frac{m^{2.24}}{\sec^{0.48} kg^{0.62}}\right) = 1.17063\times10^{-4}\left(\frac{m^{2.24}}{\sec^{0.48} kg^{0.62}}\right)$$

Regression rate analysis

Simplified approach - A simplification that is often used is to assume the regression rate only depends on the oxidizer mass flux.

$$\frac{dr\left(t\right)}{dt} = a_o \left(\frac{\dot{m}_{ox}\left(t\right)}{\pi r^2} \right)^n$$

Separate variables.

$$\frac{\pi^n}{a_o} r^{2n} dr = \left(\dot{m}_{ox}\left(t\right) \right)^n dt$$

Integrate

$$r\left(t\right) = \left(r(0)^{2n+1} + \left(2n+1\right) \frac{a_o}{\pi^n} \int_0^t \dot{m}_{ox}\left(t'\right)^n dt' \right)^{\frac{1}{2n+1}}$$

$$\frac{\dot{m}_{port}}{\dot{m}_{ox}} = \frac{\dot{m}_f + \dot{m}_{ox}}{\dot{m}_{ox}} = 1 + \left(\frac{2\pi^{1-n} a_o \rho_f}{\dot{m}_{ox}^{1-n} \left(r(0)^{2n+1} + (2n+1) \frac{a_{ox}}{\pi^n} \int_0^t \dot{m}_{ox}(t')^n dt' \right)^{\frac{2n-1}{2n+1}}} \right) x$$

In this approximation the radius at any moment is constant along the port. This assumption underpredicts the fuel generation rate and is not an accurate predictor of the O/F ratio at the end of the port especially for low O/F ratios.

The problem with a_o

The basic regression rate law can be put into the form of the simplified relation using the definition of the O/F ratio.

$$O/F = \dot{m}_{ox} / \dot{m}_f$$

$$\frac{\partial r(x,t)}{\partial t} = \frac{a}{x^m}\left(\frac{\dot{m}_{port}}{\pi r^2}\right)^n =$$

$$\frac{a}{x^m}\left(\frac{\dot{m}_{ox}\left(1+1/\left(\dot{m}_{ox}/\dot{m}_f(x,t)\right)\right)}{\pi r^2}\right)^n = \frac{a(1+1/(OF(x,t)))^n}{x^m}\left(\frac{\dot{m}_{ox}}{\pi r^2}\right)^n$$

The "constant" a_o actually depends on time and space.

$$a_o = a(1+1/(OF(x,t)))^n$$

STANFORD
AERONAUTICS & ASTRONAUTICS

Solve the nonlinear coupled mass-flow-regression-rate problem

The regression rate equation is

$$\frac{\partial r(x,t)}{\partial t} = a\frac{\dot{m}_{port}^{n}}{\pi^{n} x^{m} r^{2n}} \qquad \dot{m}_{port} = \dot{m}_{ox} + \dot{m}_{f}$$

The mass flow rate increase along the port is determined by the rate at which mass is swept up from the fuel surface.

$$\frac{\partial \dot{m}_{port}(x,t)}{\partial x} = 2\pi^{1-n} a \rho_{f} \frac{\dot{m}_{port}^{n}}{x^{m} r^{2n-1}}$$

These first order PDEs need to be solved simultaneously for the local mass flow rate and port radius.

The case $n=1/2$

The coupled problem can be solved exactly for the case $n = 1/2$.

$$r(x,t) = \left(r(x,0)^2 + \frac{2a}{x^m \pi^{1/2}} \left(\int_0^t \dot{m}_{ox}(t')^{1/2} dt' + \frac{\pi^{1/2} a \rho_f x^{1-m} t}{1-m} \right) \right)^{1/2}$$

$$\dot{m}_{port}(x,t) = \left(\dot{m}_{ox}(t)^{1/2} + \frac{\pi^{1/2} a \rho_f x^{1-m}}{1-m} \right)^2$$

The increase in port surface area exactly balances the decrease in mass flux and so the mass flow rate is constant with time for constant oxidizer mass flow rate. The O/F at the end of the port is constant.

Numerical solution of the coupled problem: variable oxidizer mass flow rate

Dimensionless variables

$$\chi = \frac{x}{r\left(0,0\right)}$$

$$0 < \chi < \frac{L_{port}}{r\left(0,0\right)}$$

$$\tau = \frac{t}{t_{burntime}}$$

$$0 < \tau < 1$$

$$R = \frac{r\left(x,t\right)}{r\left(0,0\right)}$$

$$\tilde{J}\left(x,t\right) = \frac{\dot{m}_{port}}{\dot{m}_{ox}\left(0\right)} = \frac{\dot{m}_{ox}\left(t\right) + \dot{m}_{f}\left(x,t\right)}{\dot{m}_{ox}\left(0\right)} =$$

$$\frac{\dot{m}_{ox}\left(0\right) + \dot{m}_{f}\left(x,t\right)}{\dot{m}_{ox}\left(0\right)} + \left(\frac{\dot{m}_{ox}\left(t\right) - \dot{m}_{ox}\left(0\right)}{\dot{m}_{ox}\left(0\right)}\right)$$

$$J\left(x,t\right) = \frac{\dot{m}_{ox}\left(0\right) + \dot{m}_{f}\left(x,t\right)}{\dot{m}_{ox}\left(0\right)}$$

$$\lambda\left(t\right) = \frac{\dot{m}_{ox}\left(t\right) - \dot{m}_{ox}\left(0\right)}{\dot{m}_{ox}\left(0\right)}$$

Dimensionless equations

$$\frac{\partial R}{\partial \tau} = C_R \frac{1}{\chi^m}\left(\frac{J+\lambda}{\pi R^2}\right)^n \qquad (11.20)$$

$$\frac{\partial J}{\partial \chi} = C_J \frac{2\pi R}{\chi^m}\left(\frac{J+\lambda}{\pi R^2}\right)^n \qquad (11.21)$$

Correction to notes

$\tau \rightarrow \chi$

where

$$C_R = \frac{a t_{burntime} \dot{m}_{ox}(0)^n}{r(0,0)^{2n+m+1}}$$

$$C_J = \frac{a \rho_f \dot{m}_{ox}(0)^{n-1}}{r(0,0)^{2n+m-2}}$$

The ranges of R *and* χ *are*:

$$0 < \chi < \frac{L_{port}}{r\,(0,0)}$$

$$0 < \tau < 1$$

Equations (11.20) and (11.21) can be integrated using a simple first order forward difference scheme.

Step 1 - Specify $r(0,0)$, L_{port}, $t_{burntime}$, and the regression rate constants, a, n, and m. Calculate C_R and C_J. If the initial port radius is not constant along the port, specify $R(\chi,0)$. If the oxidizer mass flow rate varies with time, specify $\lambda(\tau)$.

Step 2 - Choose a grid of χ and τ coordinates.

$$\begin{aligned} \chi_i &= (i/i_{\max})\left(L_{port}/r(0,0)\right), \quad i = 1,\ldots,i_{\max} \\ \tau_j &= (j/j_{\max}), \quad \mathrm{j} = 1,\ldots,j_{\max} \end{aligned} \tag{11.25}$$

Step 3 - Create tables defining the initial port geometry, $R(\chi_i,0)$, $i = 1,\ldots,i_{\max}$, and oxidizer mass flow rate values, $\lambda(\tau_j)$, $j = 1,\ldots,j_{\max}$.

Step 4 - Create tables defining the initial values of the radius and mass flow functions.

$$\begin{aligned} R(\chi_i,\tau_j) &= R(\chi_i,0), \quad i = 1,\ldots,i_{\max}, \quad j = 1,\ldots,j_{\max} \\ J(\chi_i,\tau_j) &= 1, \quad i = 1,\ldots,i_{\max}, \quad j = 1,\ldots,j_{\max} \end{aligned} \tag{11.26}$$

Step 5 - Update the R and J tables over the length of the port and for the length of the burn using the following first-order iterative scheme.

$$R\left(\chi_i, \tau_{j+1}\right) = R\left(\chi_i, \tau_j\right) + \Delta\tau \frac{C_R}{{\chi_i}^m} \left(\frac{J\left(\chi_i, \tau_j\right) + \lambda\left(\tau_j\right)}{\pi R(\chi_i, \tau_j)^2} \right)^n$$

$$J\left(\chi_{i+1}, \tau_j\right) = J\left(\chi_i, \tau_j\right) + \Delta\chi \frac{C_J\left(2\pi R\left(\chi_i, \tau_j\right)\right)}{{\chi_i}^m} \left(\frac{J\left(\chi_i, \tau_j\right) + \lambda\left(\tau_j\right)}{\pi R(\chi_i, \tau_j)^2} \right)^n \tag{11.27}$$

$$i = 1, \ldots, i_{\max} - 1$$

$$j = 1, \ldots, j_{\max} - 1$$

where the differences in time and space are

$$\begin{aligned} \Delta\tau &= 1/j_{\max} \\ \Delta\chi &= \left(1/i_{\max}\right)\left(L_{port}/r\left(0,0\right)\right). \end{aligned} \tag{11.28}$$

The resulting tables of $R\left(\chi_i, \tau_j\right)$ and $J\left(\chi_i, \tau_j\right)$ can be used to generate all of the information needed to characterize the burn.

Example - 100 second burn time

$n = 0.62$

$m = 0.015$

$a = 9.27 \times 10^{-5}\, m^{2.39} kg^{-0.62}\ \text{sec}^{-0.38}$

$\dot{m}_{ox} = 4.43 kg/\text{sec}$

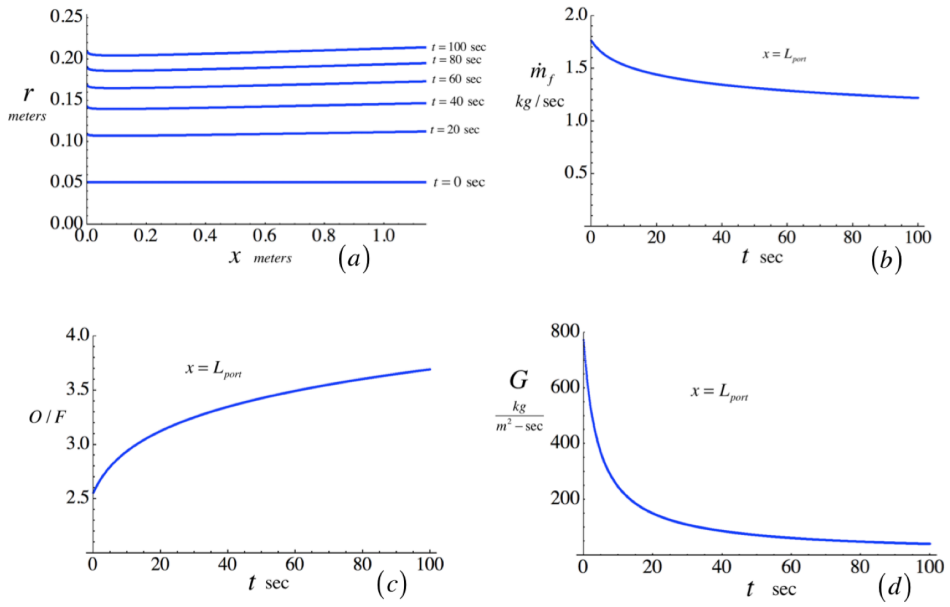

Figure 11.16: *Port functions during a 100 sec burn; (a) Port radius as a function of x at several times during the burn; (b) Fuel mass flow as a function of time at the downstream end of the port; (a) Oxidizer to fuel ratio as a function of time at the downstream end of the port; (b) Mass flux as a function of time at the downstream end of the port.*

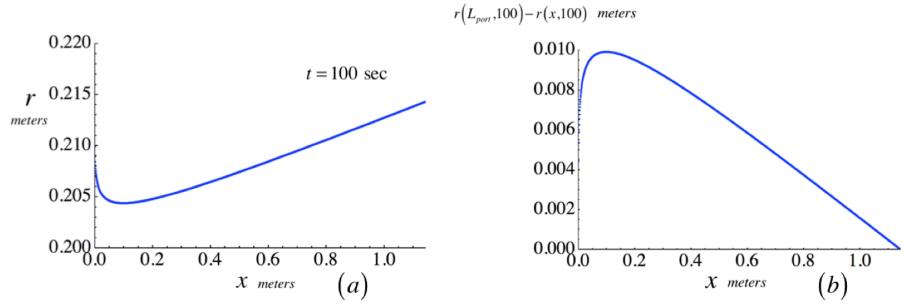

Figure 11.17: *Port functions during a 100 sec burn; (a) Close-up of the port radius function of x at the end of the burn; (b) Unburned fuel sliver at the end of the burn.*

Numerical solution captures the "coning" effect due to the mass flow increase in the port as well as the port minimum due to a nonzero *m* exponent on *x*.

STANFORD
AERONAUTICS &
ASTRONAUTICS

Paraffinic vs Polymeric Fuels

Classical Hybrids

The hybrid design concept has been known for more than 85 years.

Small hybrid rocket motors built to military specifications were used in target drone programs between 1968 and 1983 (Sandpiper, Hast, Firebolt). Eventually Space Ship Two will begin to take tourists to the edge of space.

Yet, despite this experience, the hybrid has never been developed to power large launch systems capable of taking a payload to orbit. Why?

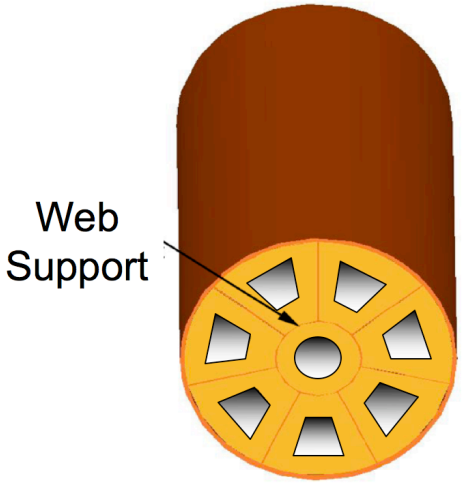

HTPB-based 7+1
Wagon Wheel

Low burning rates of polymeric fuels require a multi-port design

Disadvantage of Classical Hybrids

The hybrid design concept has been known for more than 50 years.

Small Hybrid rocket motors built to military specifications were used in target drone programs between 1968 and 1983 (Sandpiper, Hast, Firebolt). The fuel used was Hydroxyl-Terminated-Polybutadiene (HTPB).

Yet, despite this experience and clear advantages, the hybrid has never been developed to power large launch systems capable of taking a payload to orbit. Why?

Low burning rates of polymeric fuels require a multi-port design

Classical polymeric fuels such as HTPB are impractical for a launch system due to low volumetric loading, poor fuel grain structural integrity, large unburned fuel sliver

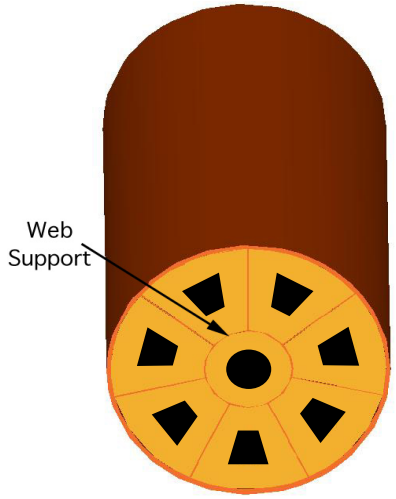

HTPB-Based
7+1 Wagon Wheel

In the early 1990's AMROC was founded to develop commercial hybrids. They tested large 250klbs thrust motors. Venture failed in the late 90's.

Lockheed Martin Michoud worked on developing a 42 port HTPB motor for use in the AF FALCON program.

Disadvantage of multiport designs

CSD (1967)
13 ports

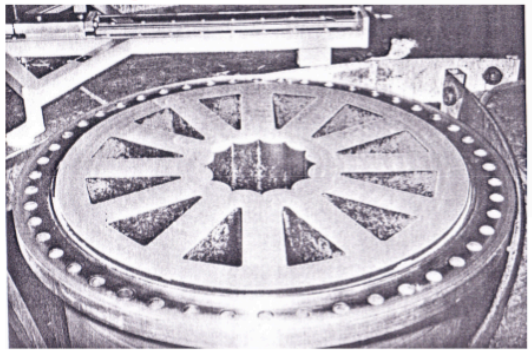

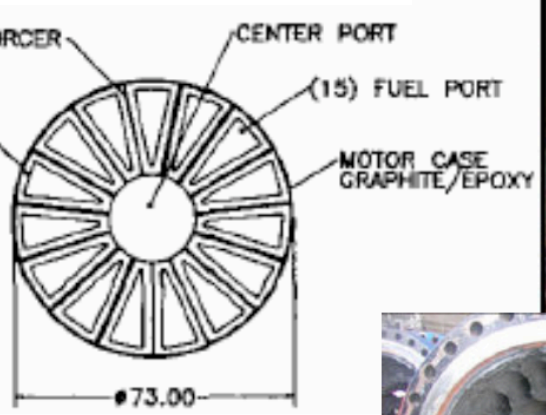

AMROC (1994)
15 ports

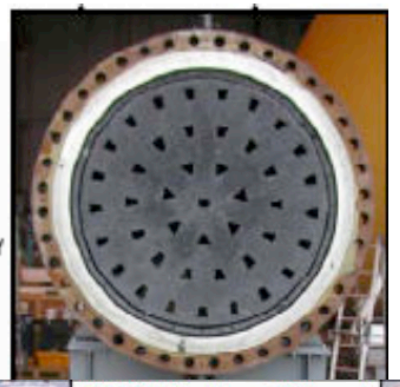

Lockheed
Martin
(2006)
43 ports

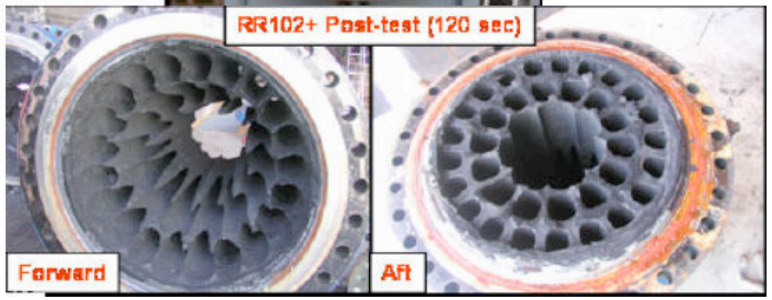

Issues with multi-port design

- *Excessive unburned mass fraction (i.e. typically in the 8% to 15% range)*
- *Complex design/fabrication, requirement for a web support structure*
- *Compromised grain structural integrity, especially towards the end of the burn*
- *Uneven burning of individual ports.*
- *Requirement for a substantial pre-combustion chamber or individual injectors for each port*

Approaches to High Regression Rate

Technique	Fundamental Principle	Shortcoming
Add oxidizing agents self-decomposing materials	Increase heat transfer by introducing surface reactions	• Reduced safety • Pressure dependency
Add metal particles (micron-sized)	Increased radiative heat transfer	• Limited improvement • Pressure dependency
Add metal particles (nano-sized)	Increased radiative heat transfer	• High cost • Tricky processing
Use Swirl Injection	Increased local mass flux	• Increased complexity • Scaling?

All based on increasing heat transfer to the fuel surface.

Solid Cryogenic Hybrids - Air Force (AFRL) Tests

- Solid propellant is a frozen material
- Motivation:
  - Performance Benefit: More flexibility on propellant selection (eg. H_2 & O_2).
- AFRL at Edwards AFB
  - Solid Pentane @ 77 K.
- 3-5 fold increase in the regression rate for pentane.

Larson, C. W., Pfeil, K. L., DeRose, M. E., and Carric, P. G., "High Pressure Combustion of Cryogenic Solid Fuels for Hybrid Rockets," AIAA Paper 96-2594, July 1996.

The Air Force shared their experimental data with us.

Entrainment Theory - Pentane Predictions

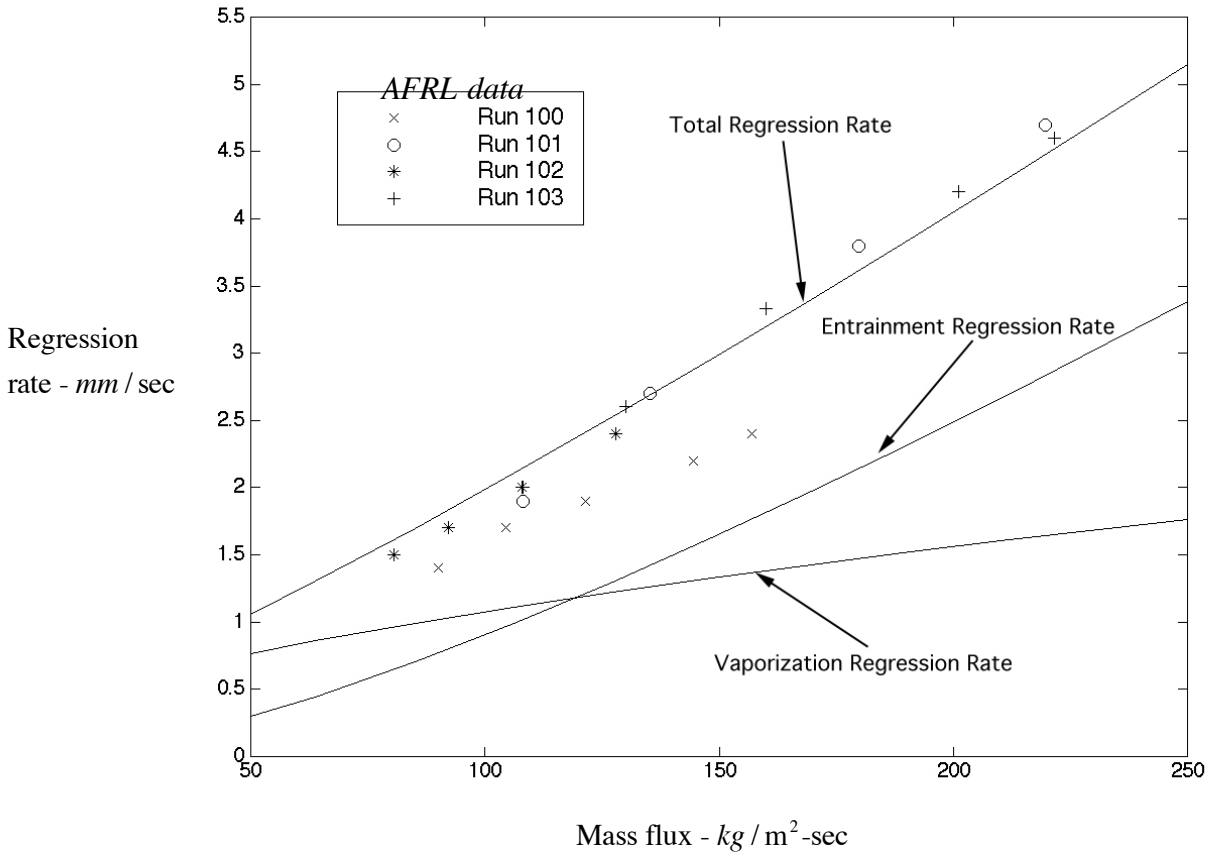

In his PhD research, Arif Karabeyoglu was able to model the high pentane mass transfer rates observed by the AFRL researchers and showed that:

1) Pentane forms a thin melt layer on the fuel surface.
2) The layer is linearly unstable under the shear by the gas flow in the port and blowing from the fuel surface.
3) Results from the Nuclear Safety literature can be used to include nonlinear growth and droplet entrainment in classical hybrid theory.

Conclusion - Total fuel mass transfer rate is increased by a factor of 3 to 4.

Thin film instability plus nonlinear growth and wave breaking leads to entrainment of droplets along the port

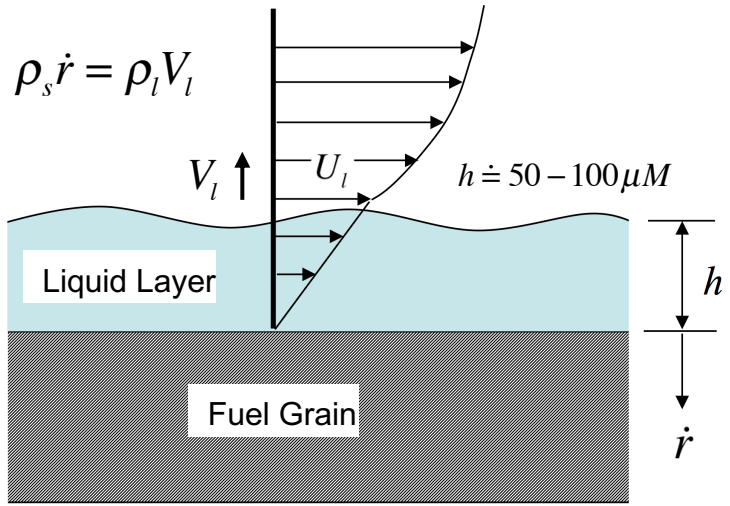

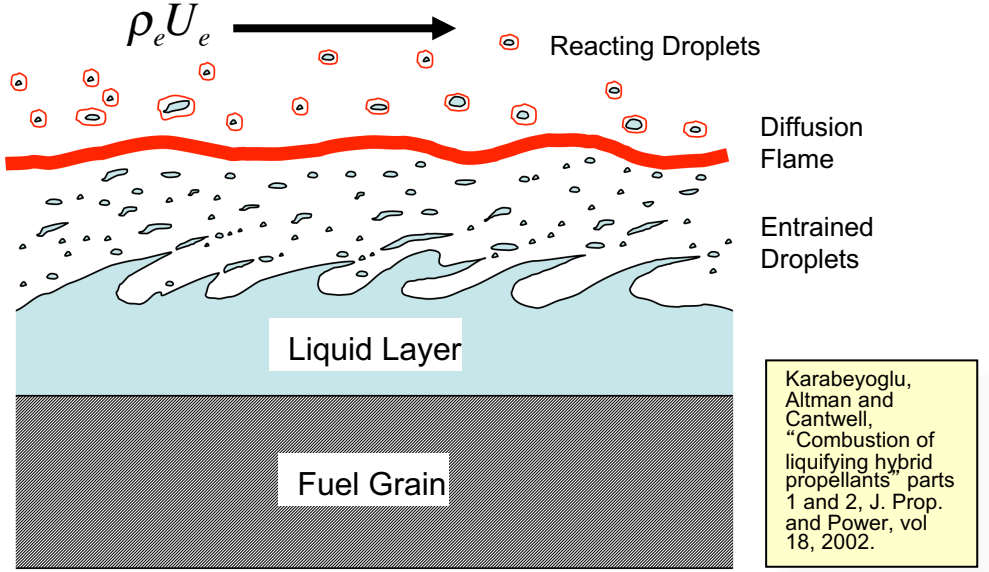

Karabeyoglu, Altman and Cantwell, "Combustion of liquifying hybrid propellants" parts 1 and 2, J. Prop. and Power, vol 18, 2002.

Film Reynolds number

$$\frac{\rho_l U_l h}{\mu_l} = 100 - 300$$

Liquid blowing Reynolds number

$$\frac{\rho_l V_l h}{\mu_l} = 0.1 - 1.0$$

Nigmatulin, R.I., Nigmatulin, B.I., Khodzhaev, D., Kroshilin, V.E., "Entrainment and Deposition Rates in a Dispersed-Film Flow" Int. J. Multiphase Flow, vol 22, 1996.

T. B. Benjamin, "Shearing flow over a wavy boundary", JFM 6, 1959.

A. D. D. Craik, "Wind-generated waves in thin liquid films", JFM 26, 1966.

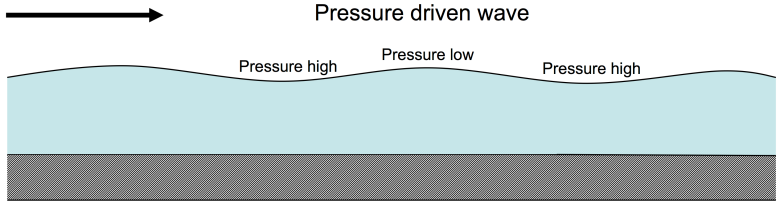

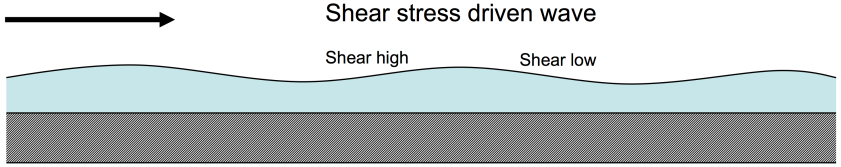

Melt Layer Temperature for C_nH_{2n+2} Series

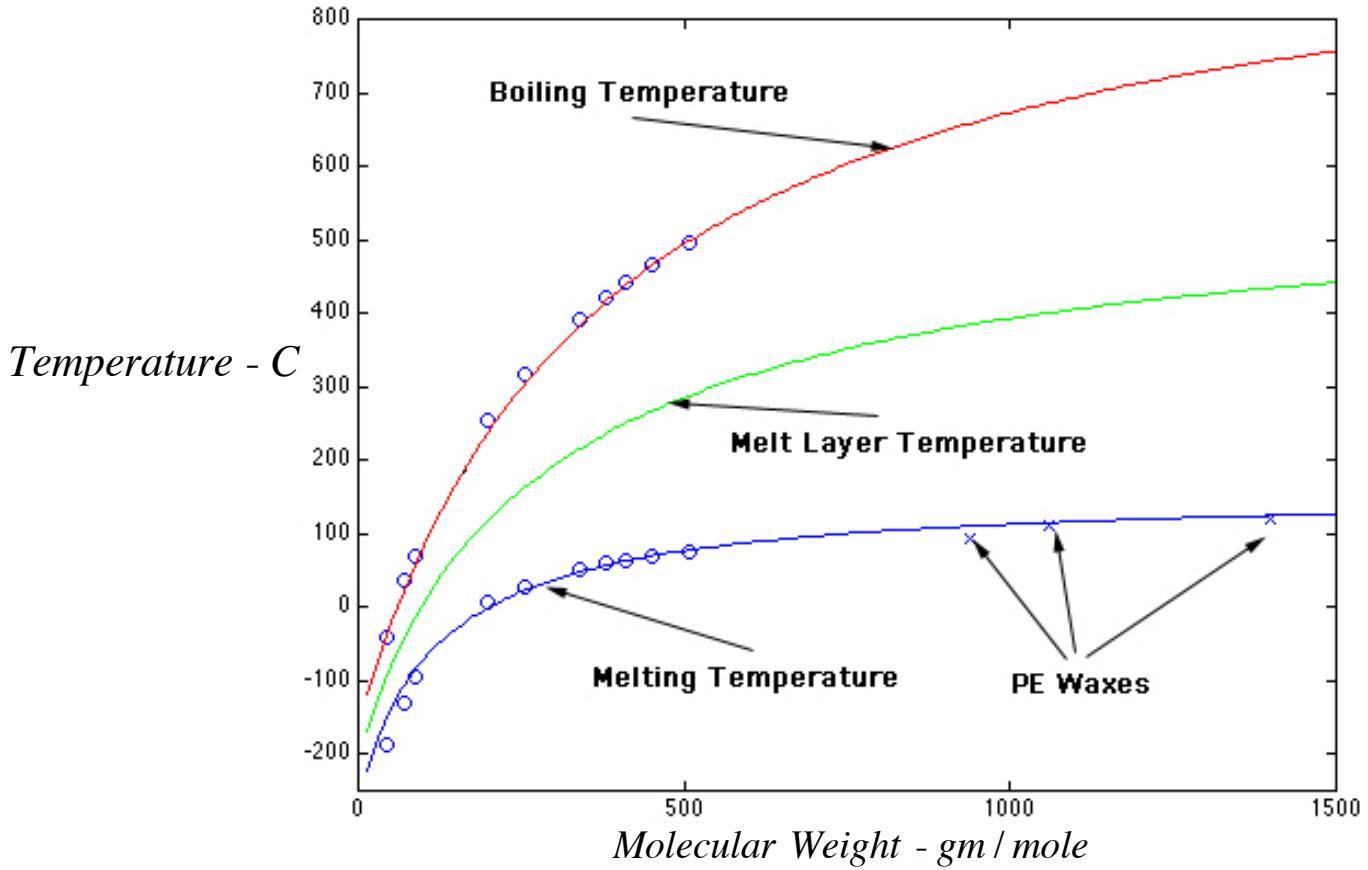

Viscosity of the melt layer increases with alkane molecular weight.

Viscosity of the melt layer decreases with melt layer temperature.

Entrainment for C_nH_{2n+2} Series

Carbon numbers between 25 and 45 are predicted to burn rapidly

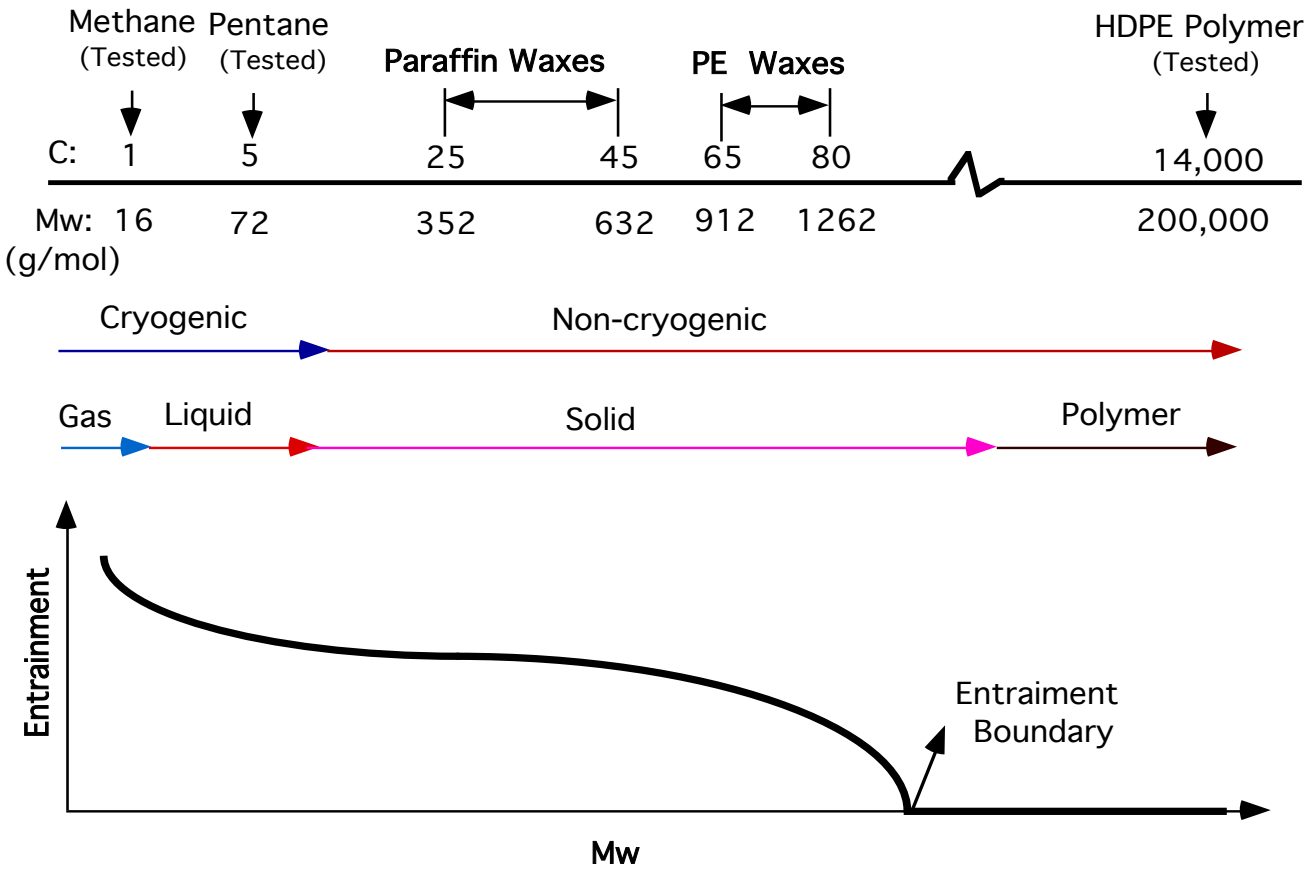

Liquid Layer Hybrid Combustion Theory

- Modify Marxman's theory to include mass transfer through droplet entrainment.

- Steps of the Theory Development
  - Estimate film thickness
  - Stability of the liquid film
  - Scaling for the entrainment mass transfer
  - Modify "Diffusion Limited Model" for the existence of entrainment
- Modification of the classical Hybrid Combustion Theory
  - Reduced heating requirement for the entrained mass.
  - Reduced "Blocking Effect" due to two phase flow.
  - Increased heat transfer due to the increased surface roughness.

Liquid layer hybrid combustion theory predicts

$$\dot{r}_{\text{"wax"}} \approx \dot{r}_{\text{pentane}} \approx 3-5 \times \dot{r}_{\text{classical}}$$

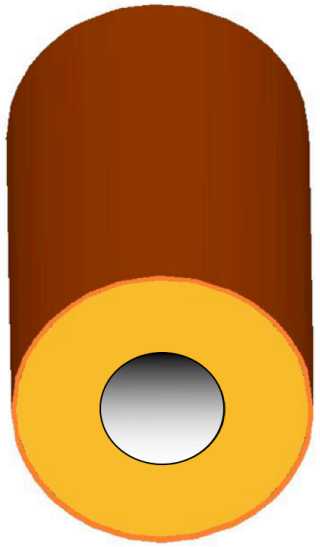

Paraffin-based
Single Circular Port

Diagram depicts an 83% fuel loading design

The high burn rate of paraffin-based fuels leads to a single port design that makes large hybrids practical.

Fuel loading above 80% is feasible

STANFORD
AERONAUTICS &
ASTRONAUTICS

NASA Ames Hybrid Combustion Facility

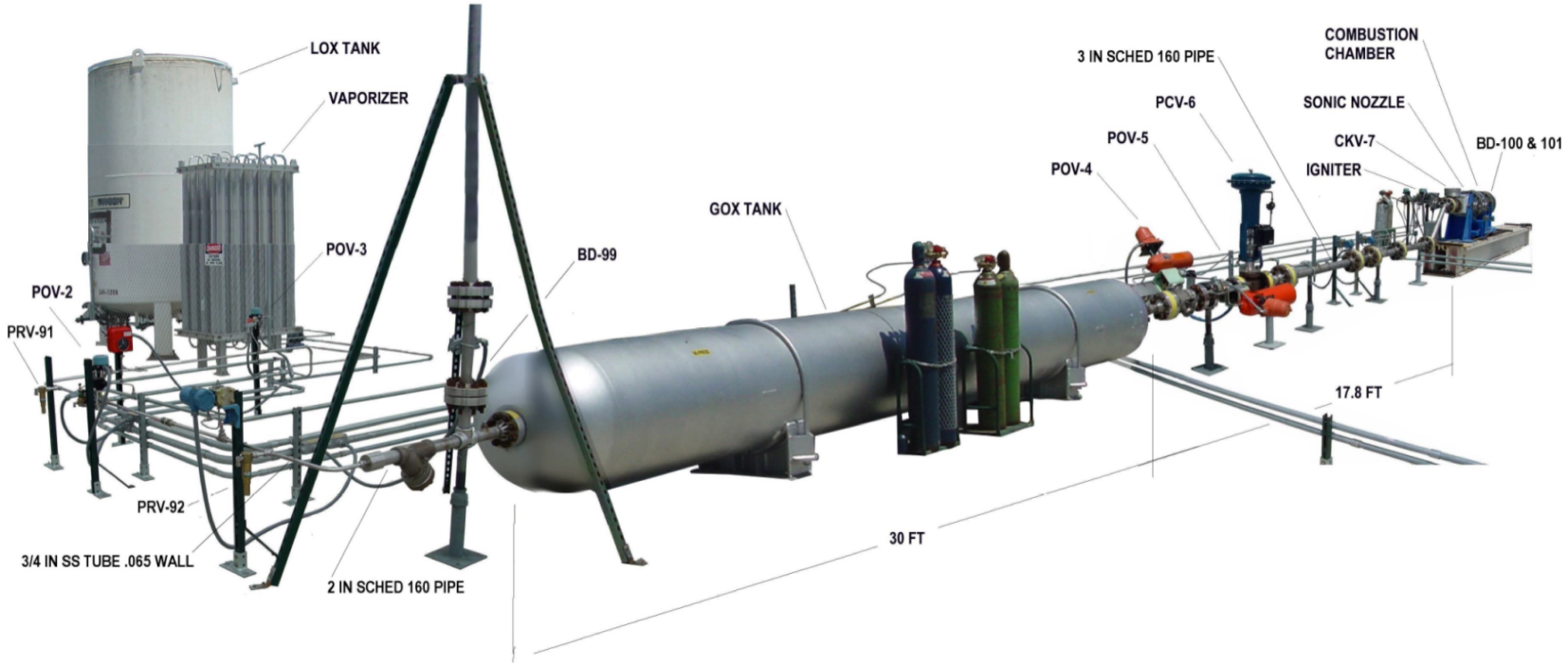

STANFORD
AERONAUTICS &
ASTRONAUTICS

Test Motor Configuration

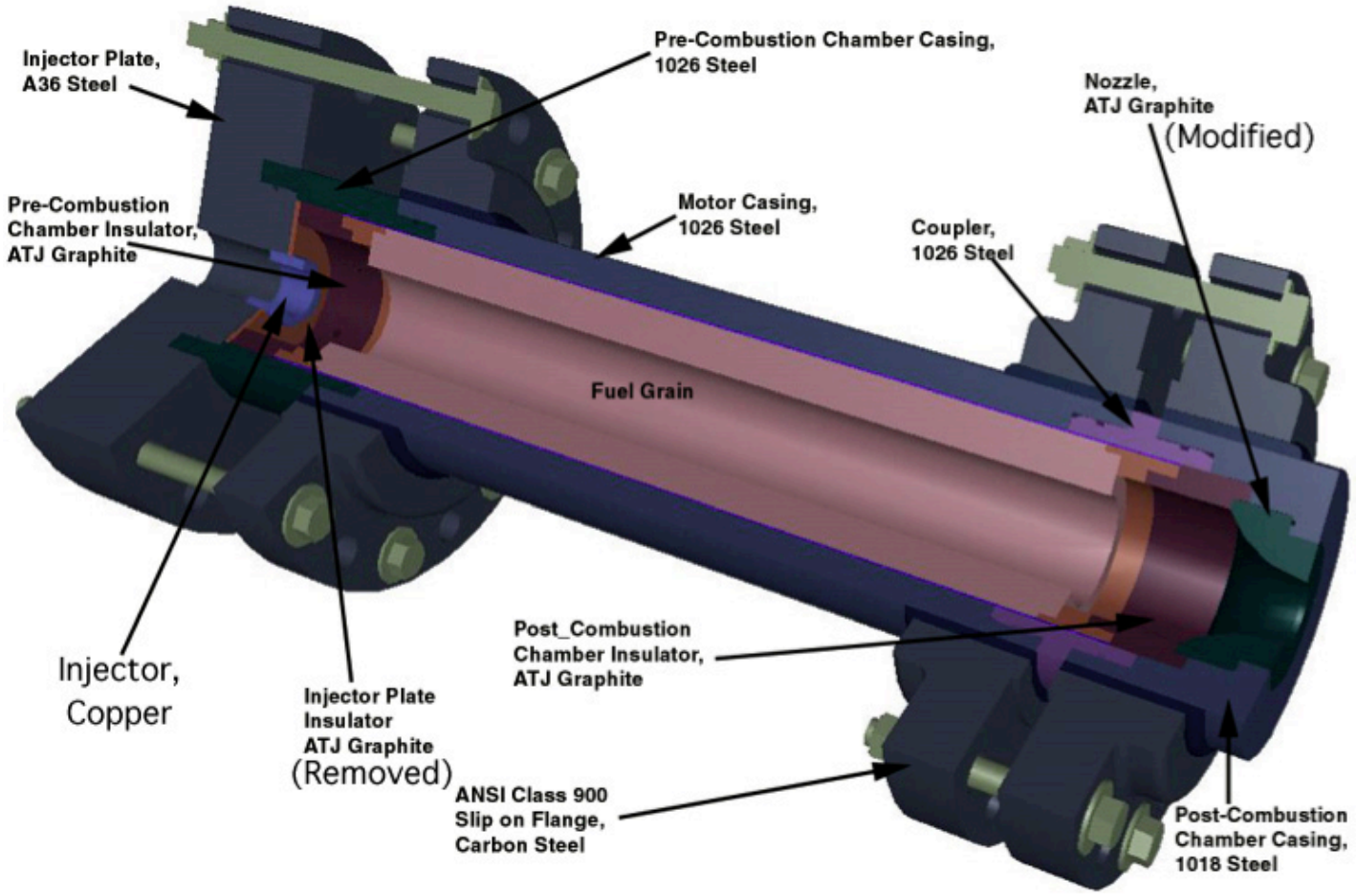

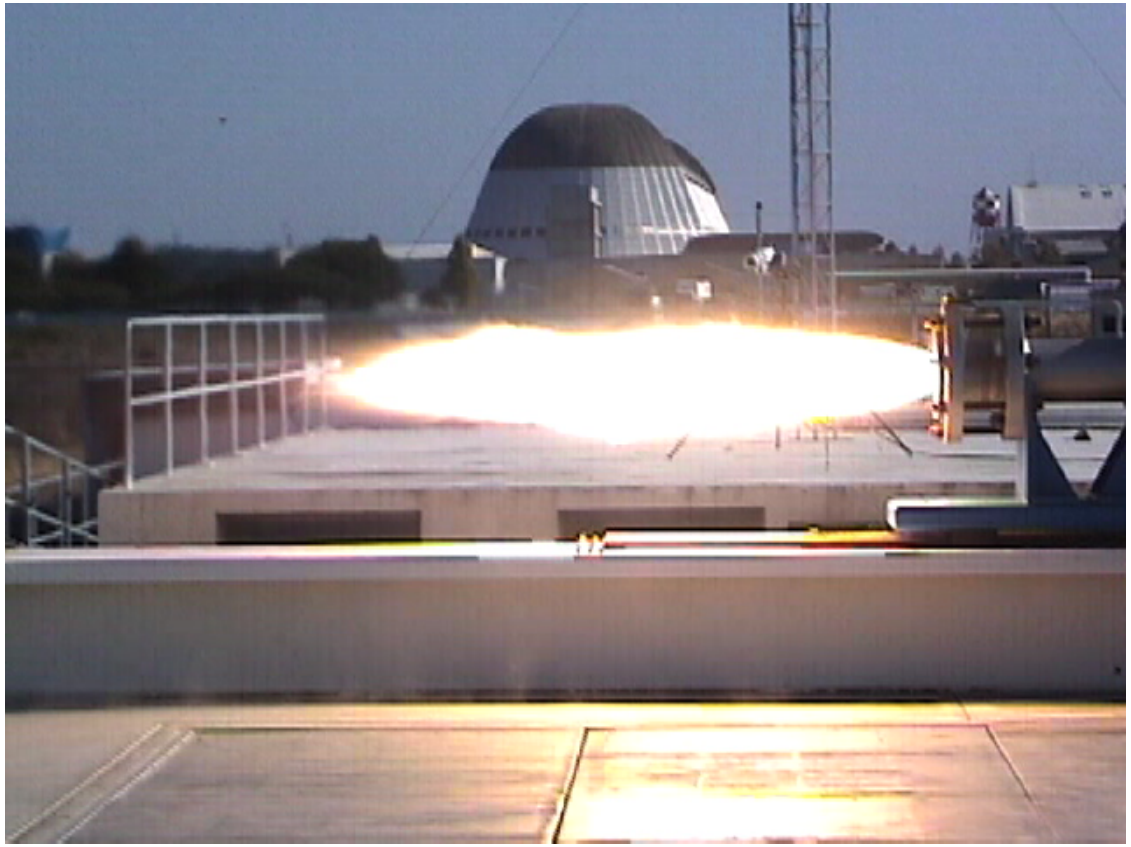

Regression rate data for paraffin-based fuel

Paraffin-based fuel: 70C Melt Point, Fully Refined Wax ($C_{32}H_{66}$) + 2% Stearic Acid ($C_{18}H_{36}O_2$) by weight

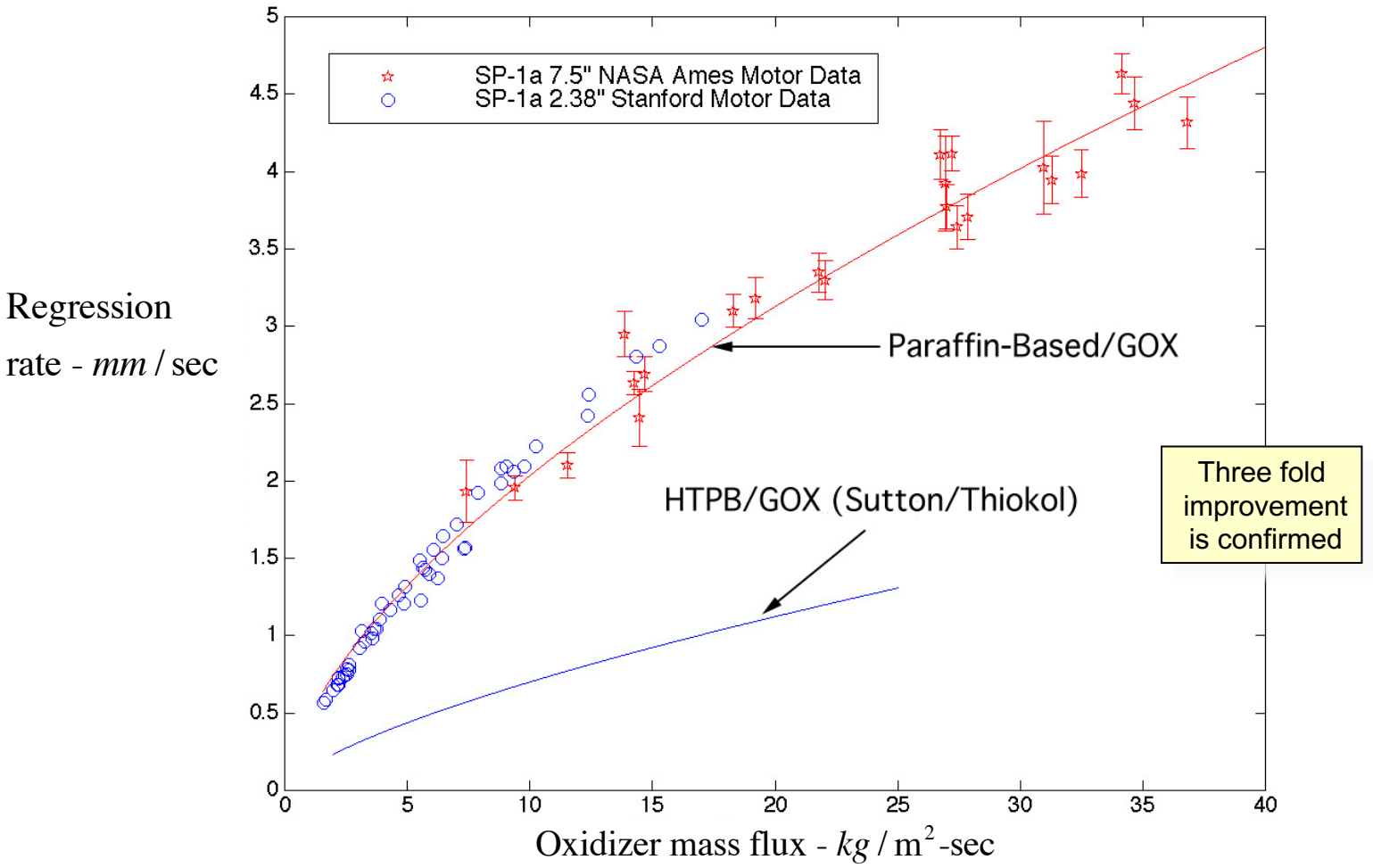

A Typical Pressure-Time History

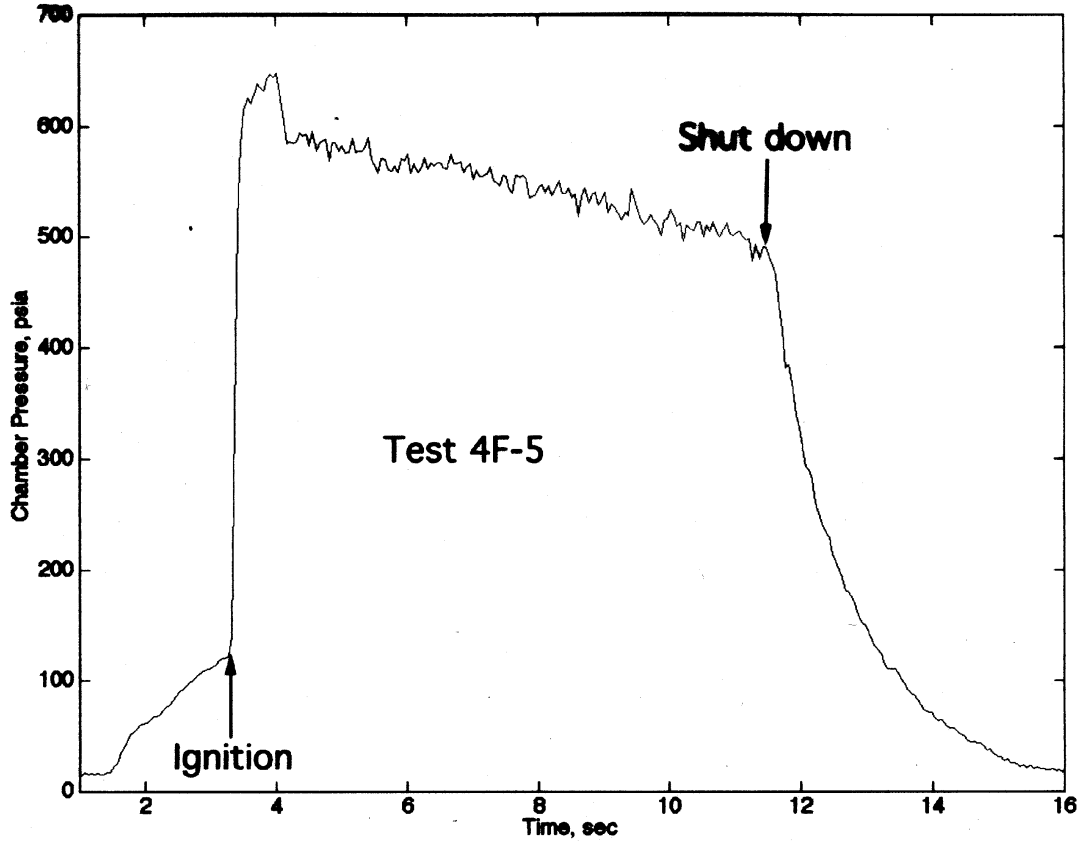

Figure 8: Chamber pressure-time trace for the run 4F-5.

Theoretical Isp Performance with LOX

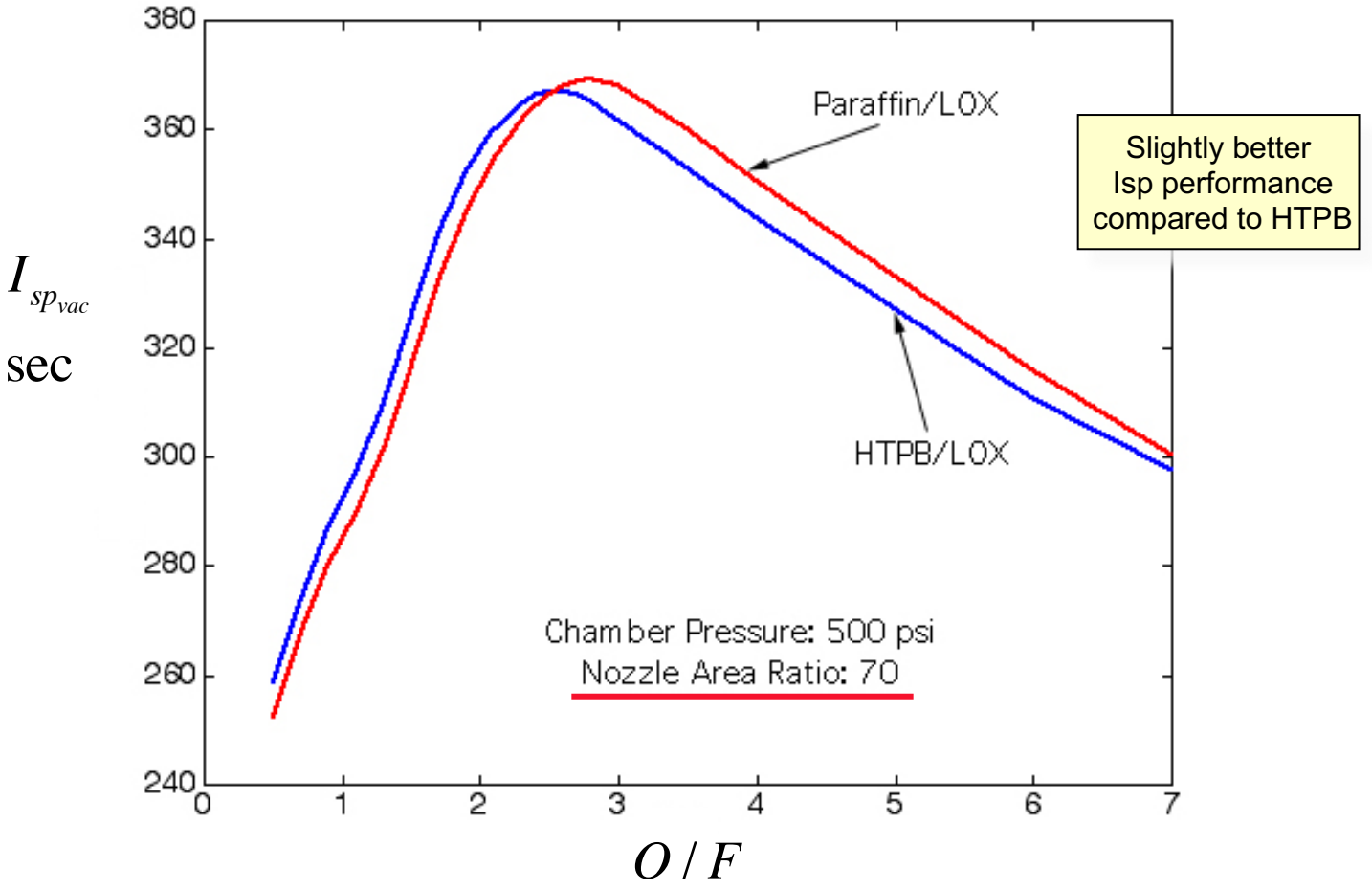

Over 1000 tests to date at several scales using single port design

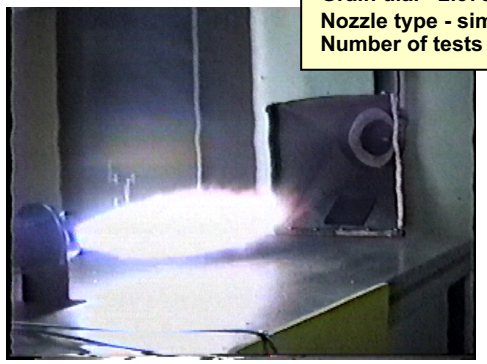

Thrust class - 50 lbs
Oxidizer - GOx
Grain dia. - 2.375 inches
Nozzle type - simple conv.
Number of tests - 300

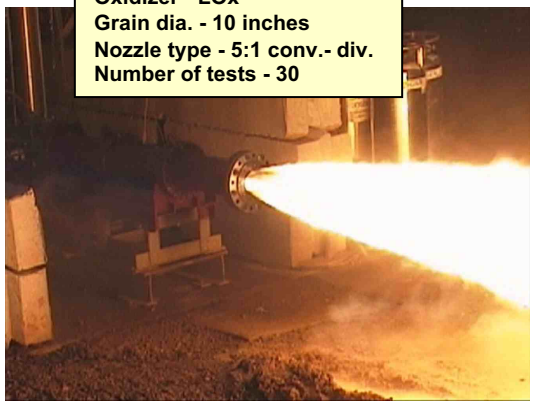

Thrust class - 6000 lbs
Oxidizer - LOx
Grain dia. - 10 inches
Nozzle type - 5:1 conv.- div.
Number of tests - 30

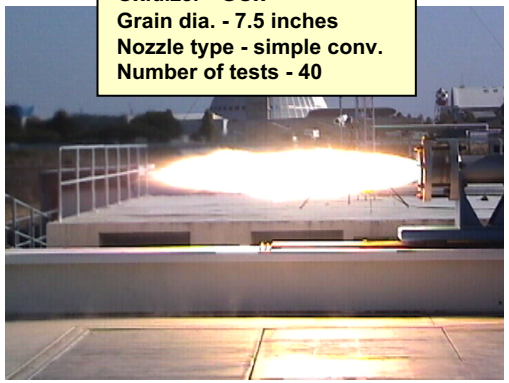

Thrust class - 2500 lbs
Oxidizer - GOx
Grain dia. - 7.5 inches
Nozzle type - simple conv.
Number of tests - 40

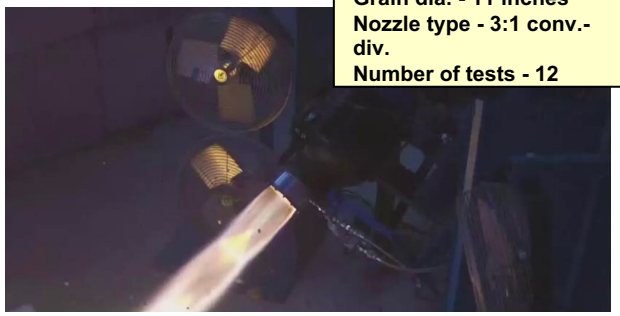

Thrust class - 2000 lbs
Oxidizer – MON3
Grain dia. - 11 inches
Nozzle type - 3:1 conv.-div.
Number of tests - 12

Thrust class - 900 lbs
Oxidizer - N2O
Grain dia. - 5.25 inches
Nozzle type - 5:1 conv.- div.
Number of tests - 15

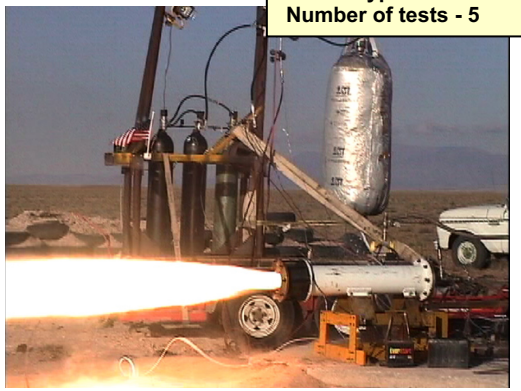

Thrust class - 3000 lbs
Oxidizer - LOx
Grain dia. - 8.4 inches
Nozzle type - 5:1 conv.-div.
Number of tests - 5

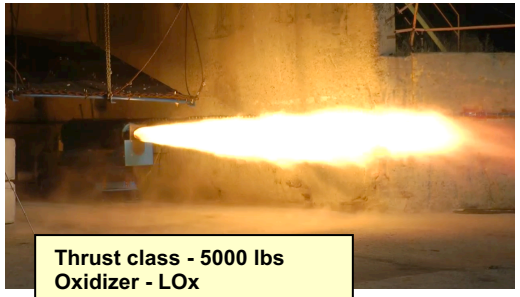

Thrust class - 5000 lbs
Oxidizer - LOx
Grain dia. - 8.4 inches
Nozzle type - 2:1 conv.-div.
Number of tests - 50

Thrust class - 15000 lbs
Oxidizer - N2O
Grain dia. - 12 inches
Nozzle type - 5:1 conv.- div.
Number of tests - 25

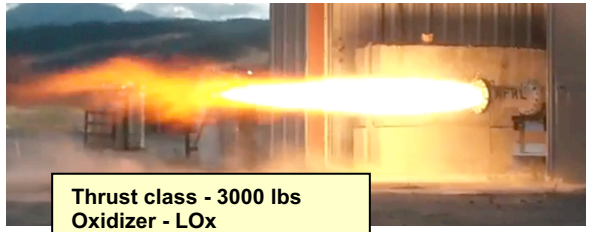

Thrust class - 3000 lbs
Oxidizer - LOx
Grain dia. - 8.4 inches
Nozzle type - 2:1 conv.-div.
Number of tests - 50

STANFORD
AERONAUTICS &
ASTRONAUTICS

FLAME VISUALIZATION

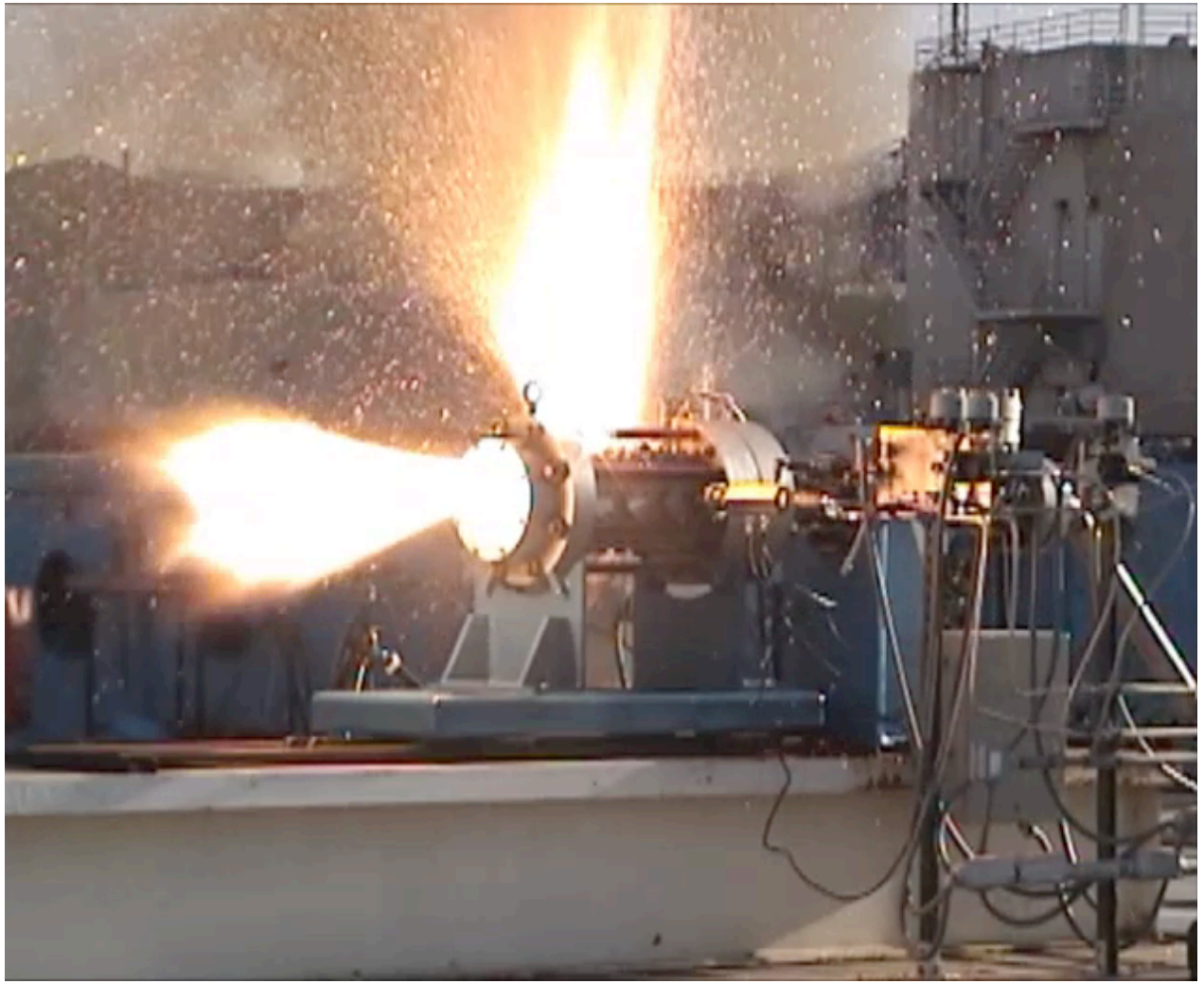

Oxygen compatible combustion visualization tunnel Ashley Karp, Beth Jens

The experimental challenge –
directly visualize oxygen-fuel combustion at 3000K up to 2 MPa

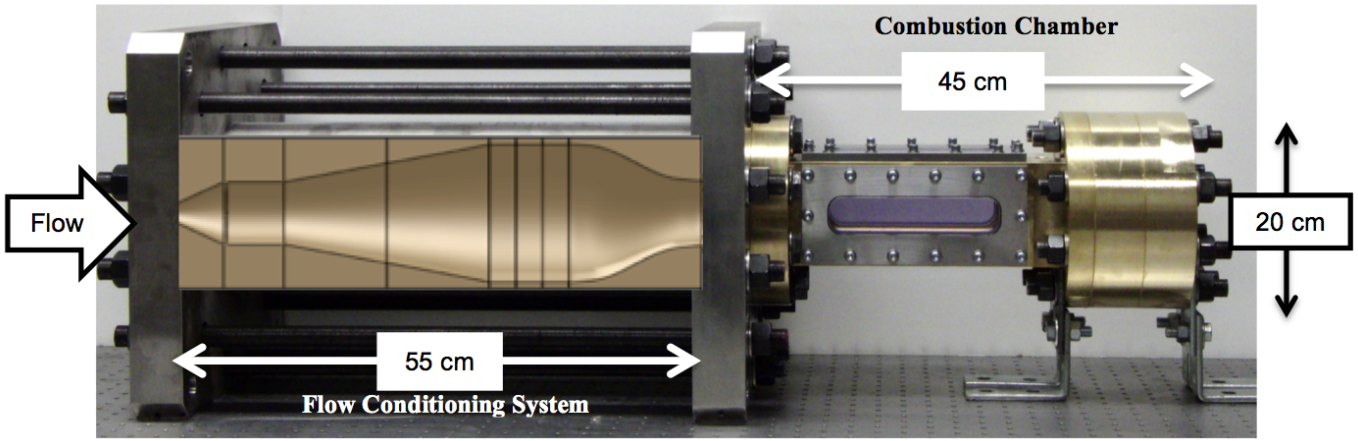

- Material - Brass
- Chamber pressure: atmospheric up to 17.24 bar
- Windows: 3.81 cm Polycarbonate, later Quartz
- Ignition: Nichrome wire, currently diode laser

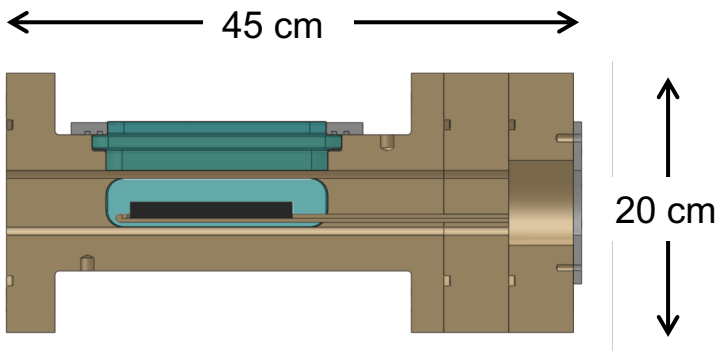

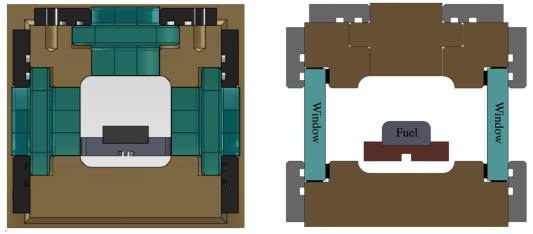

STANFORD
AERONAUTICS &
ASTRONAUTICS

The burn time for each test is 3 - 7 seconds

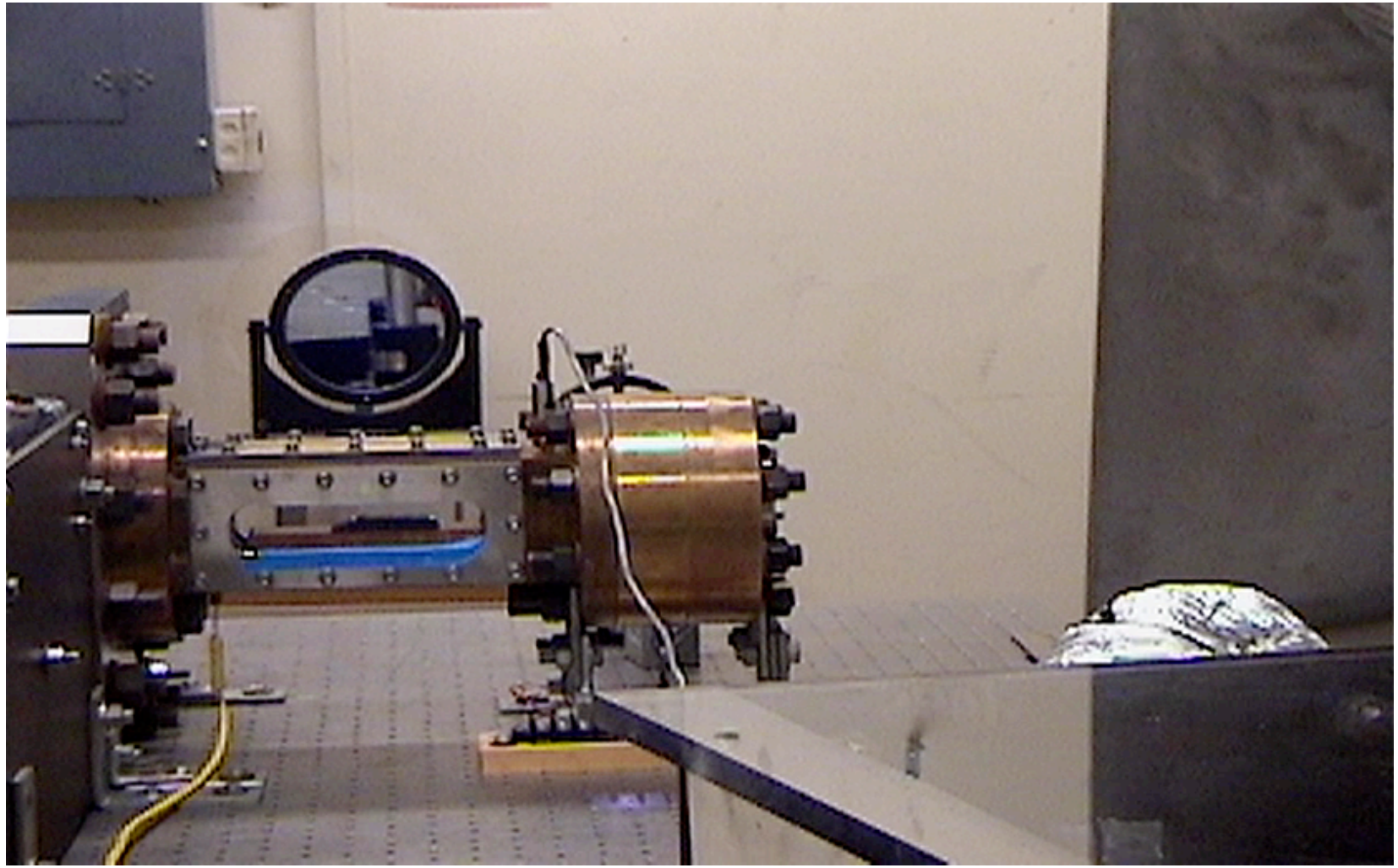

Combined schlieren and OH* results - Blackened Paraffin 71 psi

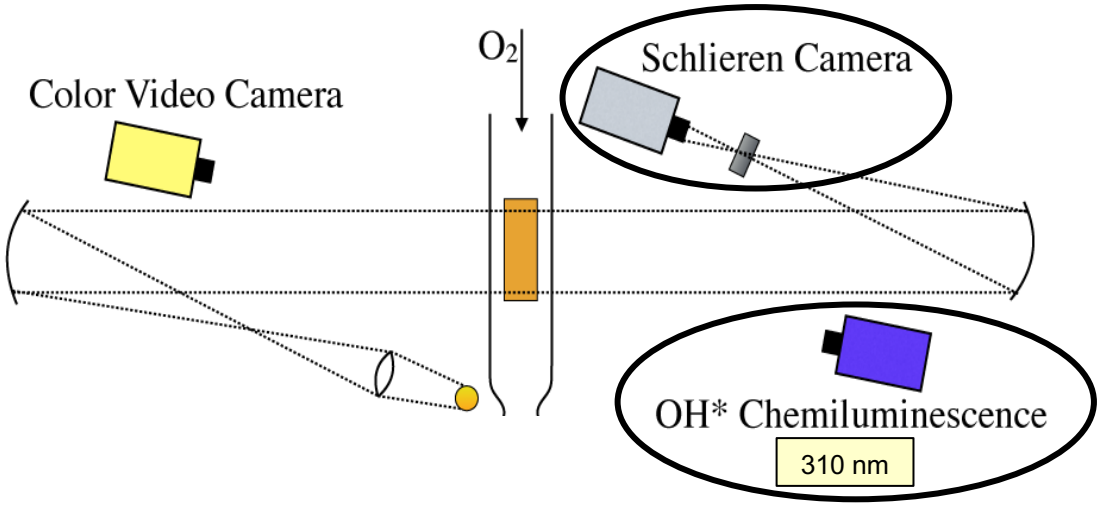

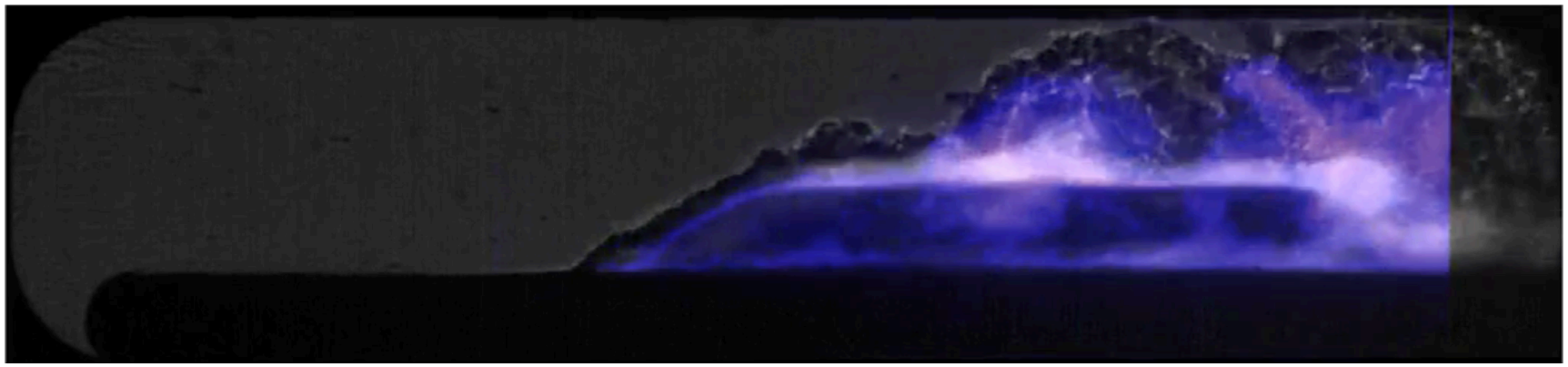

Jens, et al.,"Schlieren and OH* chemiluminescence imaging of combustion in a turbulent boundary layer over a solid fuel " *Experiments in Fluids*, 57:39, March 2016.

Elevated pressure blackened paraffin tests – 170 psi

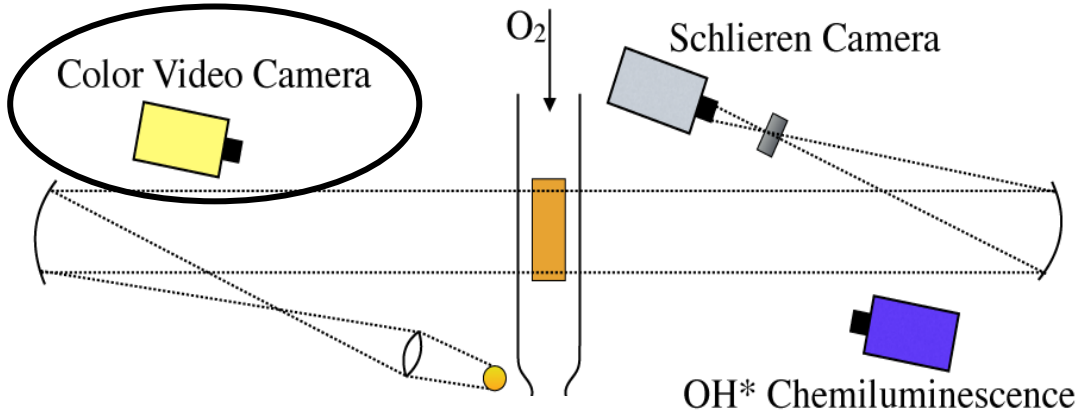

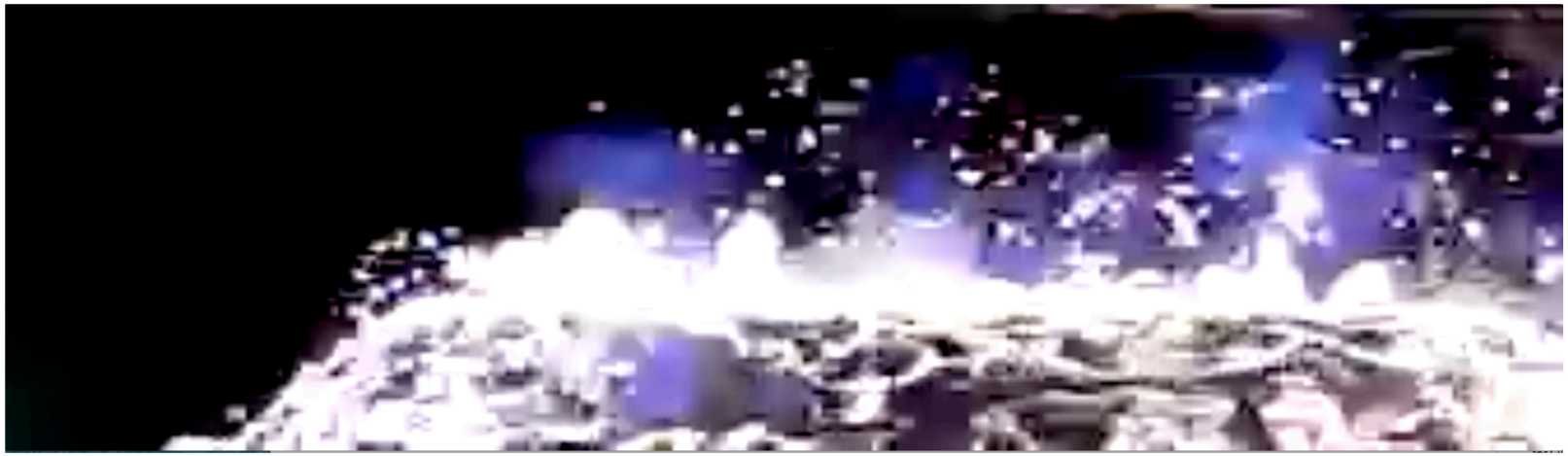

Elevated pressure blackened paraffin tests

G_{OX} = 20.5 kg/m^{2}s

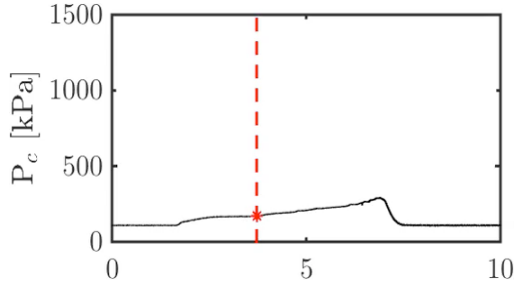

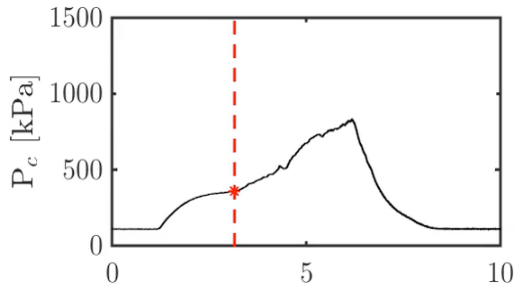

G_{OX} = 36.4 kg/m^{2}s

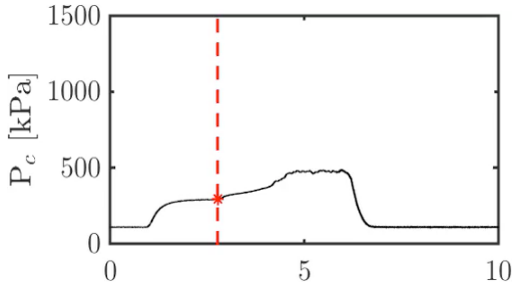

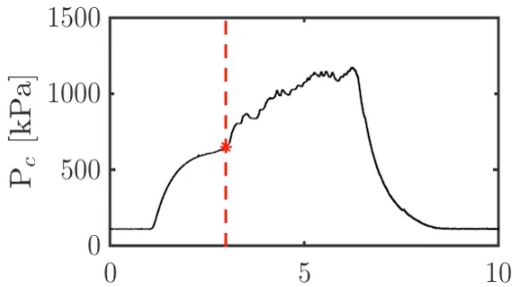

The largest motor we have built to date is a 15,000 lb class motor for the Peregrine sounding rocket project led by Greg Zilliac of NASA Ames

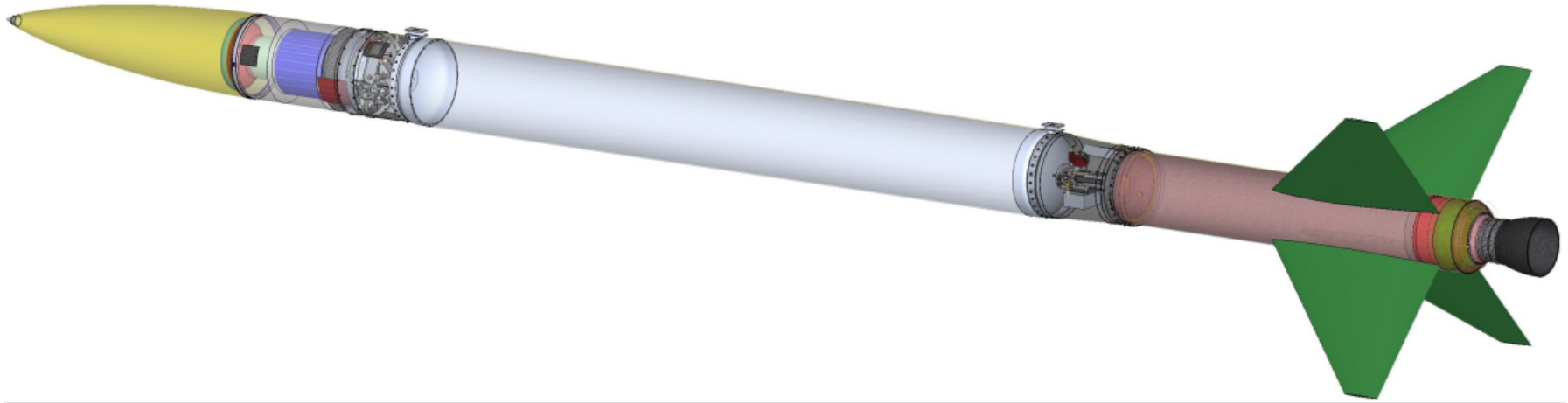

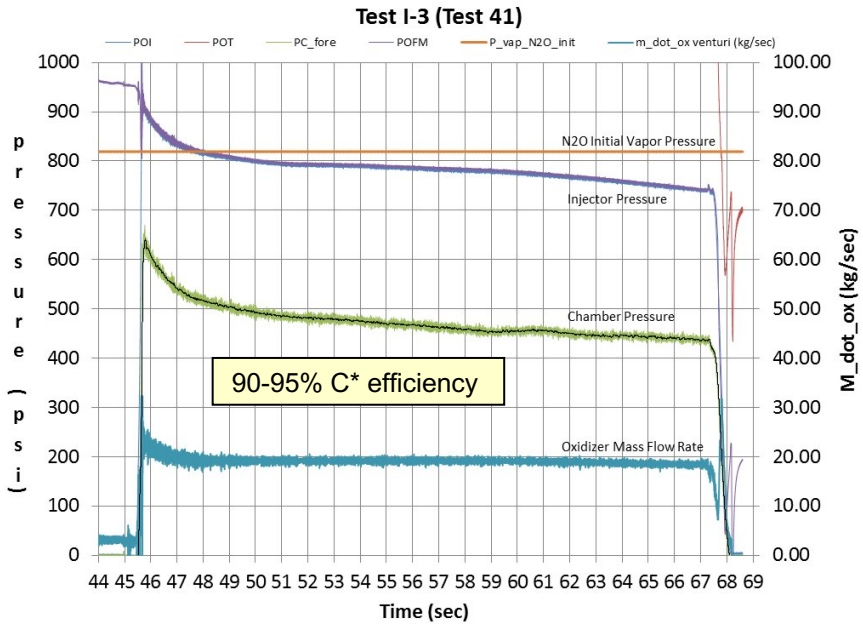


NASA

Applications

Launch boosters, small satellite launch

In-space motors

- Orbit changing, planetary exploration

Sub-orbital space flight

- Space tourism - Space Ship One, Space Ship Two

Science and Technology Missions

- Zero gravity experiments
- Sounding rockets - A large number of very low cost solid systems are available but they restrict the kinds of payloads that are flown. NASA runs 30 to 40 flights per year
- Planetary exploration

STANFORD
AERONAUTICS &
ASTRONAUTICS

The Mars Ascent Vehicle

$$GLOM = 400kg$$

$$Length = 2.80m$$

$$Diameter = 0.57m$$

$$Orbit = 300km$$

$$\Delta V = 3900m/\sec$$

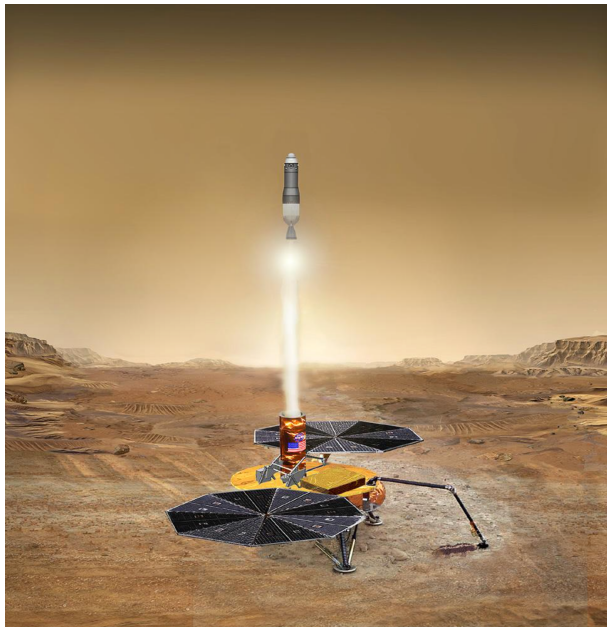

MSR Mission Architecture

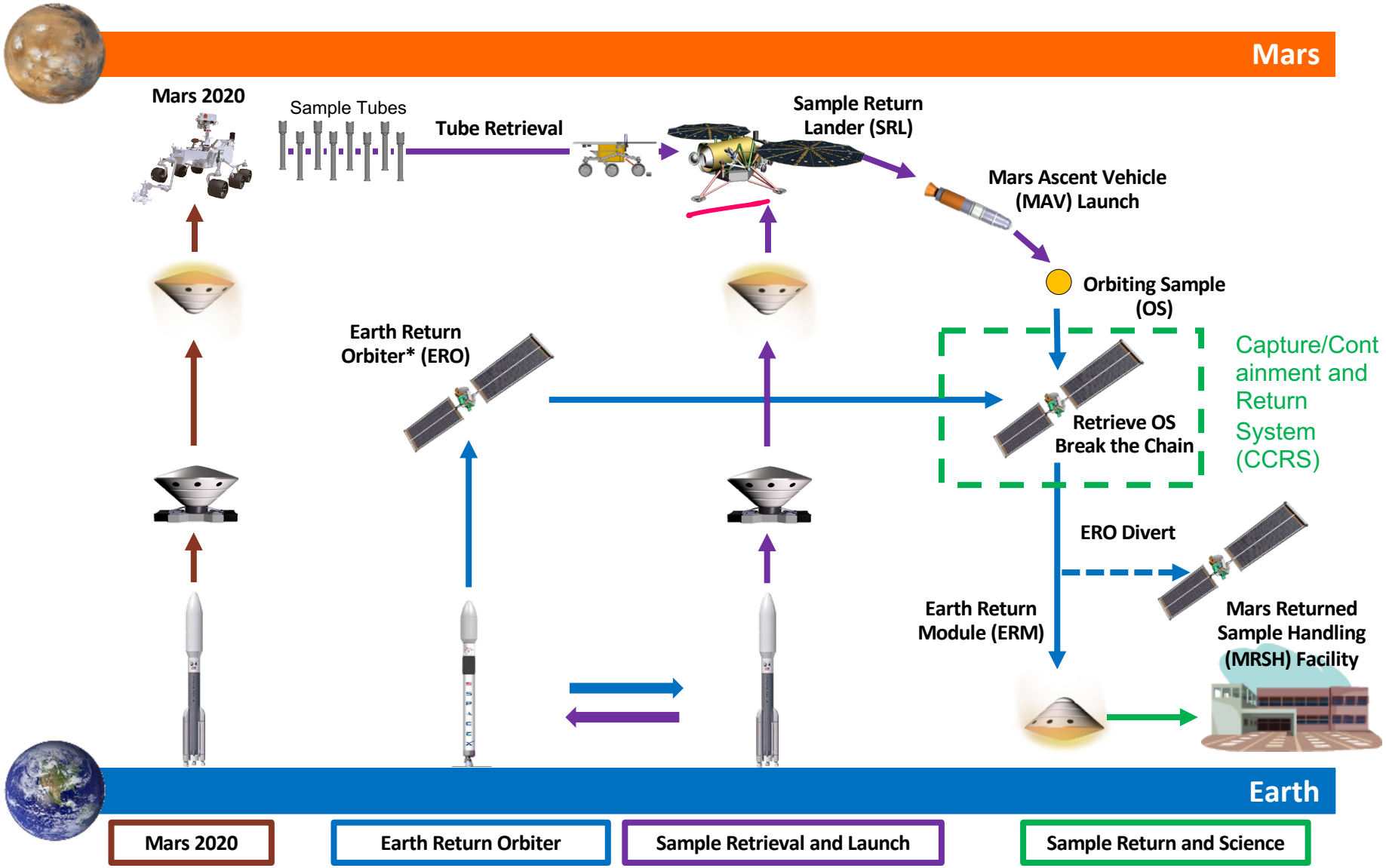

Orbiting Sample (OS)

The Mars 2020 rover will drill rock samples and place them in individual tubes.

The samples would be left on the surface of Mars for later pick up by a second rover.

The second rover would place the samples in the payload bay of the MAV which would then launch to Mars orbit.

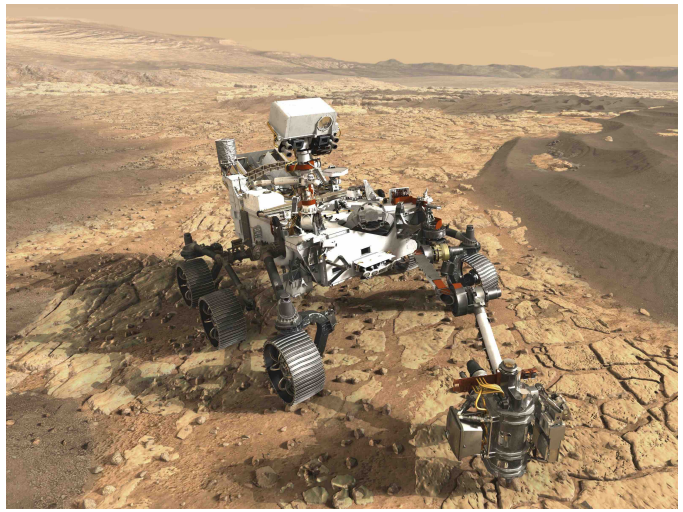

Current OS
Reference Design

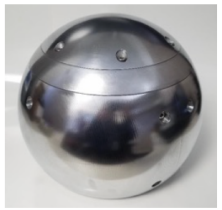

Engineering OS ready for
impact testing

Mars 2020 Sample Tube
Assembly

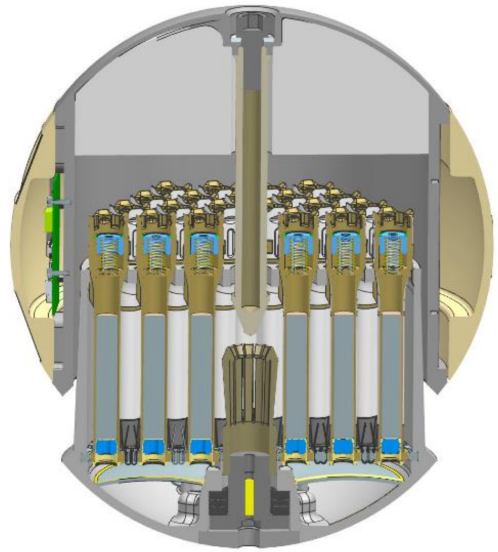

Mars 2020 landing site was chosen November 2018

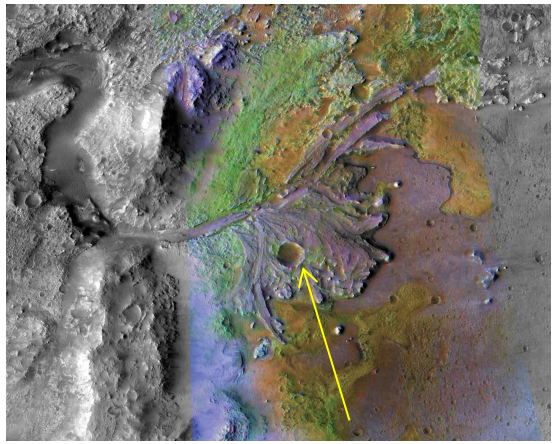

Jezero crater - 18° above the Mars equator

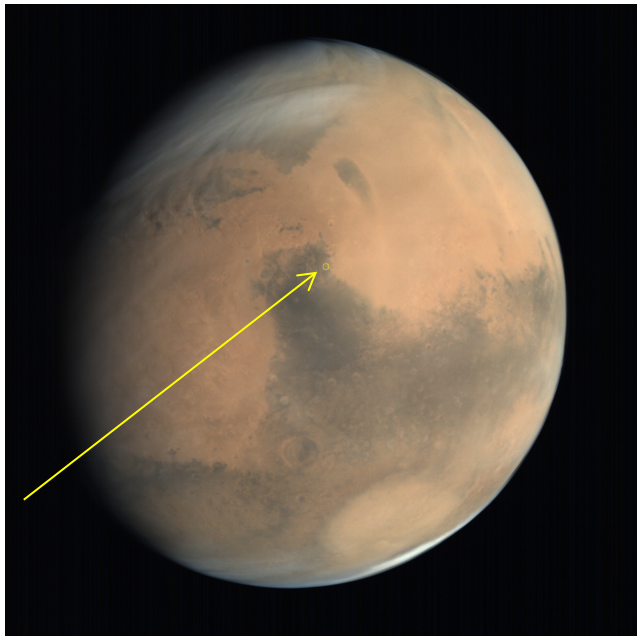

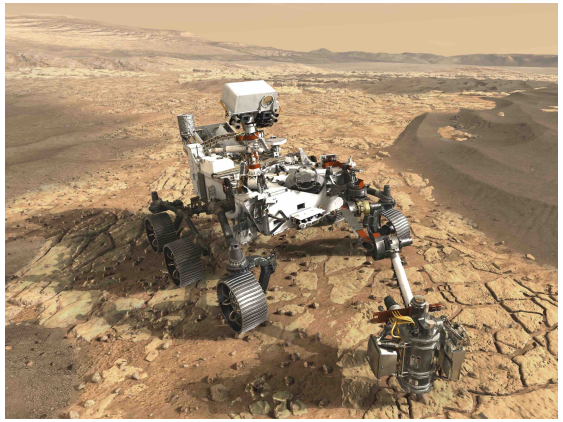

Curiosity rover – Temperature and Pressure at Gale crater on Mars (Aug 2012 to Feb 2013

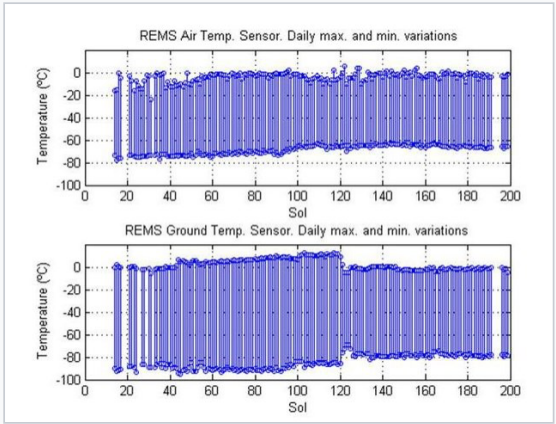

Temperature

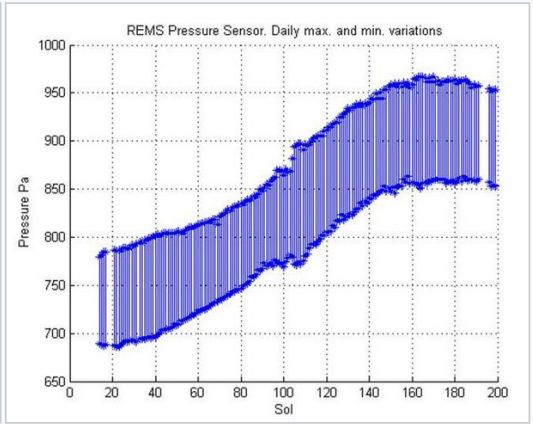

Pressure

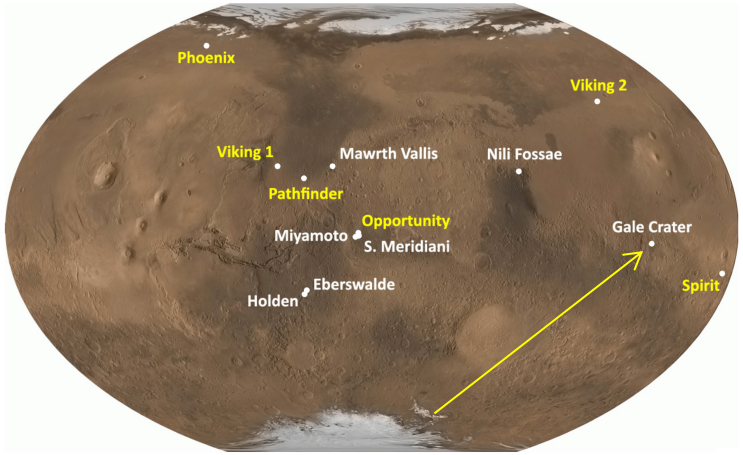

Gale crater - 5° below the Mars equator

Fuel temperature predictions during the Martian year including EDL

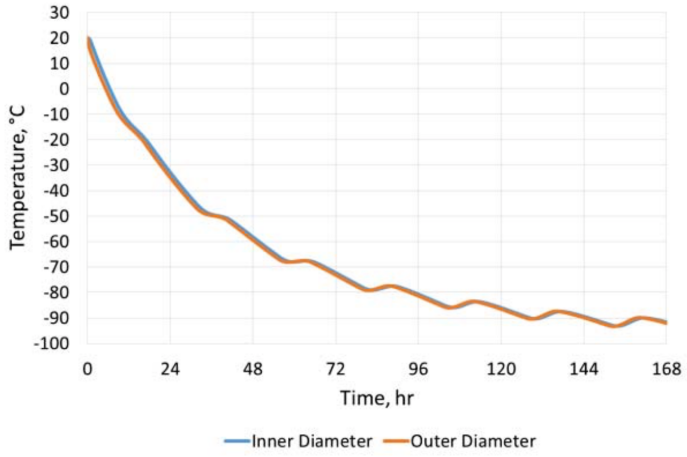

a. EDL

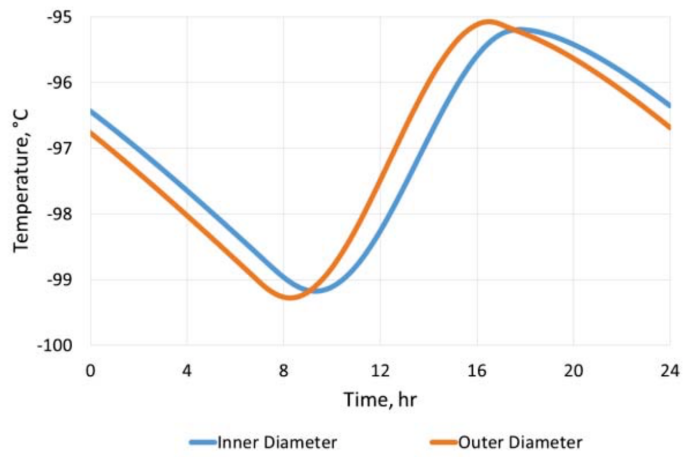

b. Winter

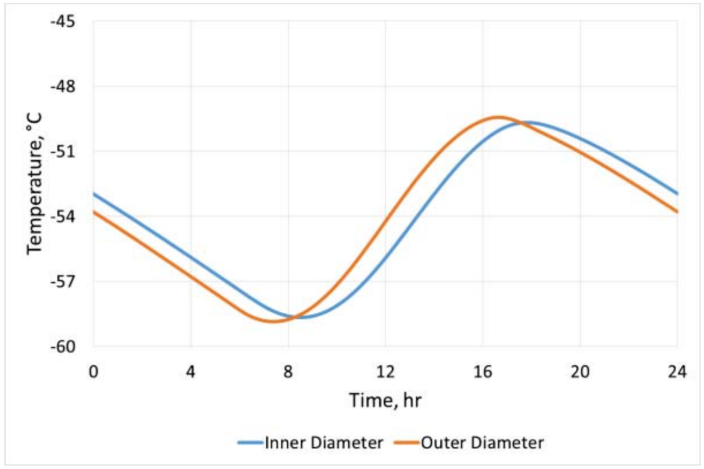

c. Spring

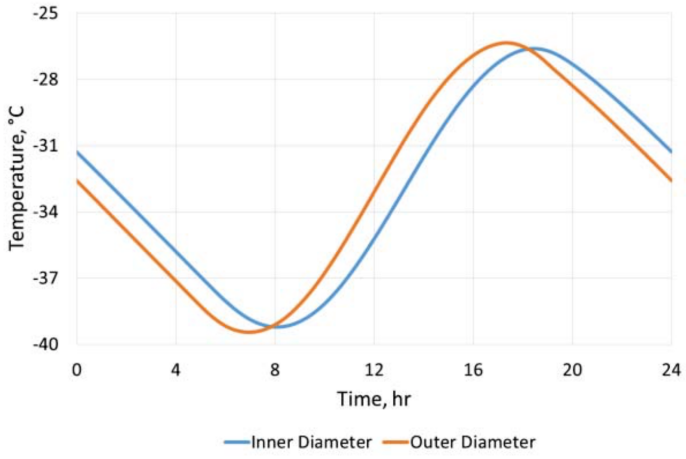

d. Summer

A wide temperature range fuel designated SP7 was developed in 2015 by Space Propulsion Group, Inc.

Thermal cycling representative of 200 Mars sols at Mars pressure was carried out at NASA Marshall Space Flight Center. Both aluminized and non-aluminized samples were studied.

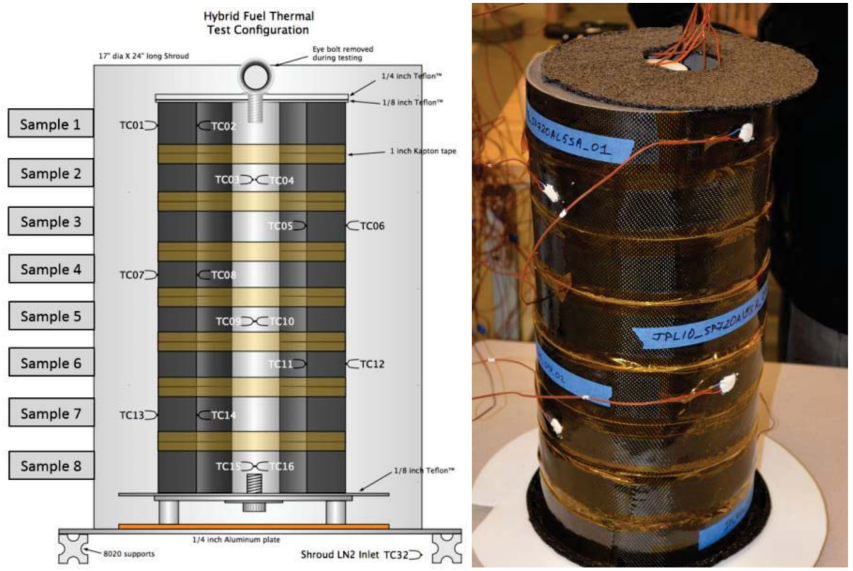

Figure 11. Test configuration for long term temperature cycling of eight SP7 fuel samples. Each fuel sample is instrumented with a thermocouple at the inner and outer diameters.

The EDL cycle and the 50 winter cycles have been completed. The samples were removed from the test chamber for inspection following the completion of the 50 winter cycles. Small cracks were observed on a couple of samples; no large radial cracks were observed. Some small cracks were visible in the circumferential direction as expected. Further testing will determine if these cracks are an issue if they propagate into larger cracks or if they can be prevented. All eight samples successfully survived the EDL and winter cycles and will continue testing with the 100 spring/fall cycles.

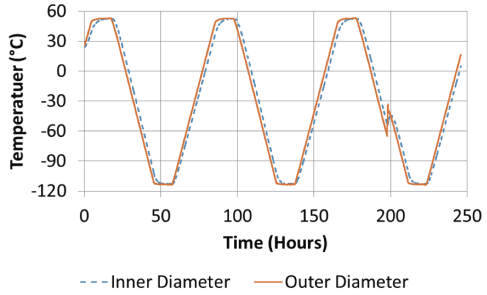

Figure 3. Temperature cycling profile for the most severe temperature cycle (+50 °C to -110 °C)

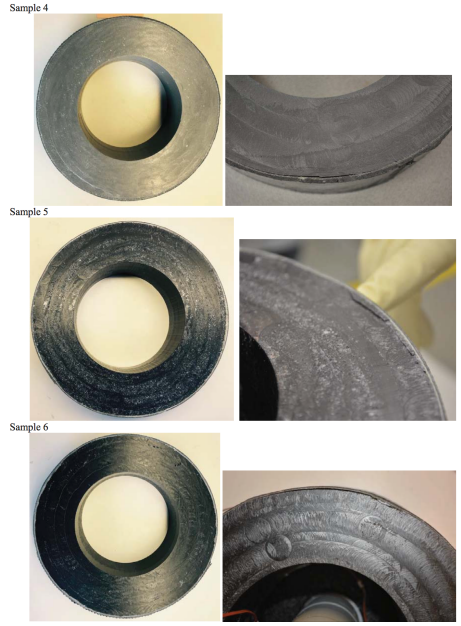

MAV Development testing

Space Propulsion Group

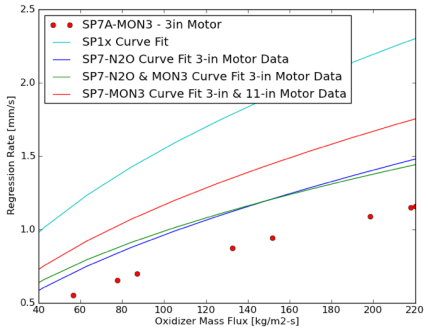

Regression Rate

Whittinghill Aerospace

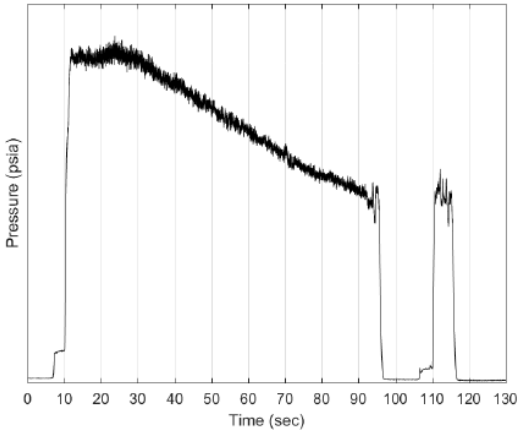

Restart

LITVC

SP7/MON-3

SP7/MON-25 at -20 C

MON3 and MON25 have a relatively low vapor pressure requiring substanial heat addition at the fore end of the motor to achieve stability. To address this a low flow of MMH is injected which is hypergolic with MON.

Hybrid SSTO MAV Design – JPL/MSFC

- Design predicted to close from a propulsion point of view (GLOM~400 kg, dV=~3900 m/s, fits in the lander)
- More development work to be done
  - No obvious show stoppers
  - Testing to demonstrate that the total impulse can be delivered
  - Some analyses need to be finalized to reduce mass
- Engine shutoff is an important capability
  - Additional capability in the RCS system for fine tuning of orbit
- Motor design is flexible and can be modified as vehicle matures
- Preliminary thermal, structural, and CFD analysis results have been incorporated
- Orbit tolerances met in all cases

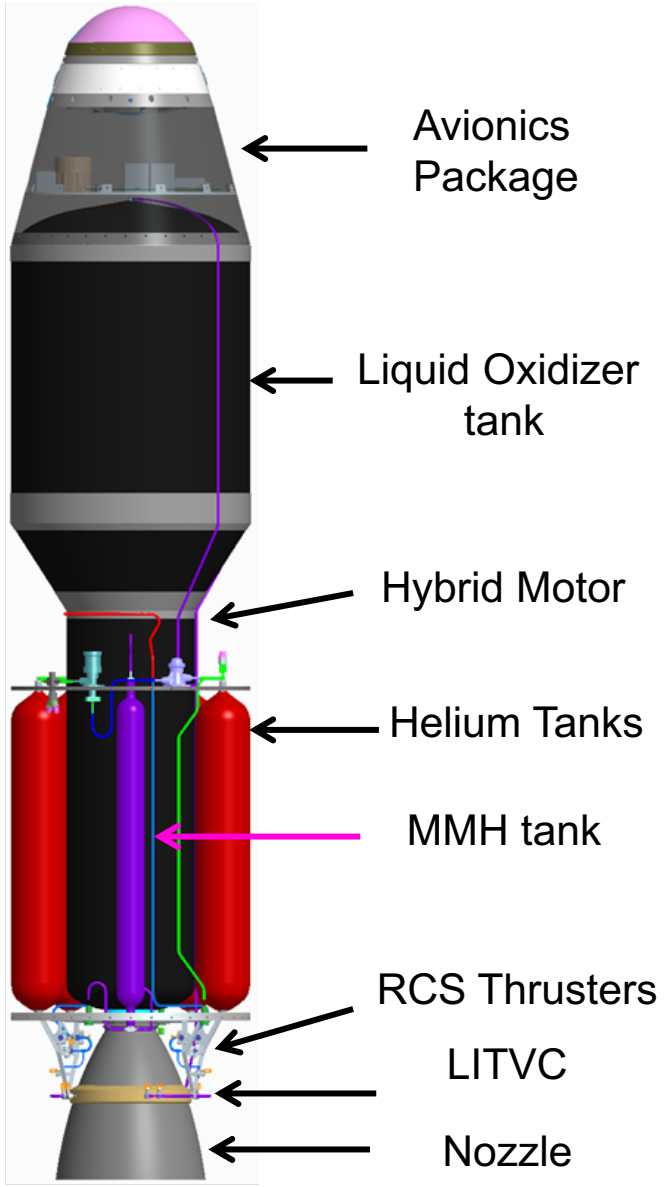

In 2018 the decision was made to to provide a thermal control system (igloo) for the MAV

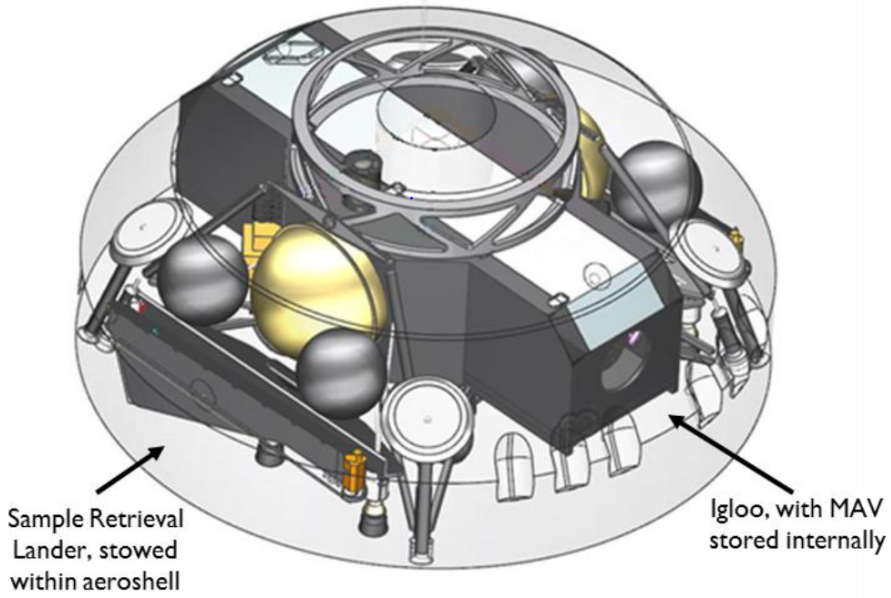

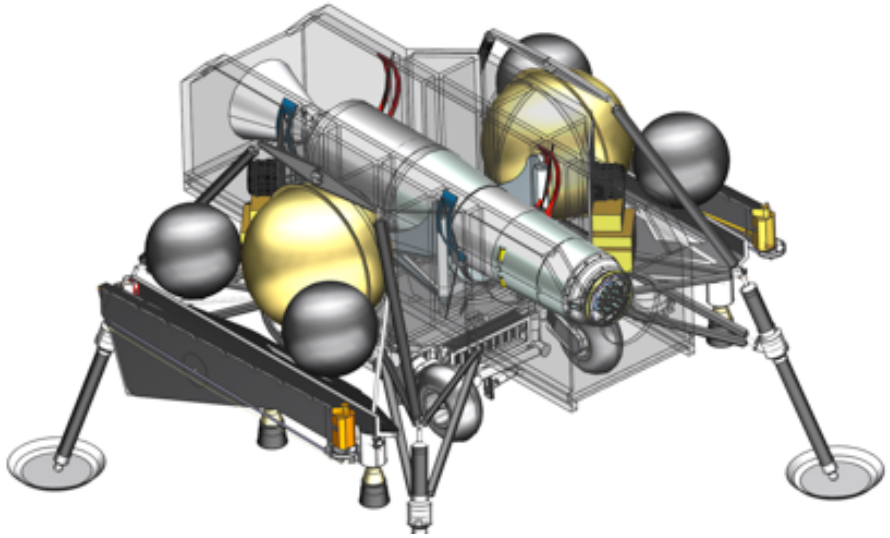

High Technology Readiness Level (TRL) Thermal control system components are used to maintain MAV operating (-20C) and non-operating (-40C to +40C) temperatures for all stages of flight.

MAV Decision late 2019

- Benefits of the hybrid option include its predicted low temperature behavior, high performance and ability to restart (enabling the SSTO).
- MAV 2015 Study concluded that for MAV low temperature requirements, hybrids had advantages. However TRL was low and a plan was made to develop the technology to be ready to compete for > 2030 launch.
- In 2018, the launch window was moved up to 2026, shortening technology development time for the hybrid.
- In 2018 decision was made to use an igloo to provide thermal control of the MAV while on the Mars surface. This increased launch temperature requirement from -50C to -20C.
- Solid option has a high TRL level. Studies are currently underway to determine if the solid can meet orbital dispersion requirements.
- Downselect between the two options occurred in late 2019 – two stage solid was selected.

AIAA Propulsion and Energy Forum
19-22 August 2019, Indianapolis, IN
AIAA Propulsion and Energy 2019 Forum

10.2514/6.2019-3840

Check for updates

A Single Stage to Orbit Design for a Hybrid Mars Ascent

George Story[1], Andrew Schnell[2], and Darius Yaghoubi[3]
NASA Marshall Space Flight Center, Huntsville, Al, 35812, USA

Ashley Karp[4], and Barry Nakazono[5]
Jet Propulsion Laboratory, California Institute of Technology, Pasadena, CA, 91109, USA

Greg Zilliac[6]
NASA Ames Research Center, Moffett Field, CA, 94035, USA

AIAA Propulsion and Energy Forum
19-22 August 2019, Indianapolis, IN
AIAA Propulsion and Energy 2019 Forum

10.2514/6.2019-4149

Check for updates

A Design for a Two-Stage Solid Mars Ascent Vehicle

Andrew Prince[1], Timothy Kibbey[2]
NASA Marshall Space Flight Center (MSFC), Huntsville, AL 35812, United States of America

Ashley Karp[3]
Jet Propulsion Laboratory (JPL), California Institute of Technology, Pasadena, CA 91109, United States of America

Two Stage Solid MAV Design – JPL/MSFC

- Solid propulsion TRL is high with a legacy of use on Mars.
- Vehicle Gross Lift-Off Mass (GLOM), temperature extremes, and orbital dispersions are the most significant challenges
- Mission design includes two burns separated by a long coast
  - Stage 1 puts the vehicle into a highly elliptical orbit with an apoapsis at the desired altitude of the circular orbit, but with a negative periapsis.
  - Once the vehicle has coasted nearly to apogee, Stage 2 fires to circularize the orbit
- RCS must conduct control maneuvers during the long coast between stages.
- Orbital dispersion currently under study